ELSEVIER

Contents lists available at ScienceDirect

International Journal of Multiphase Flow

journal homepage: www.elsevier.com/locate/ijmulflow





Experimental study of bubble growth on novel fin structures during pool boiling

Mahyar Ghazvini ^a, Mazen Hafez ^a, Philippe Mandin ^b, Myeongsub Kim ^{a, a}

- ^a Ocean and Mechanical Engineering, Florida Atlantic University, 777 Glades Rd., Boca Raton, FL 33431
- ^b Institut de Recherche Dupuy de Lôme, UMR CNRS 6027, 56100 Lorient, France

ARTICLE INFO

Keywords: Thermal Management Nucleate Boiling Bubble Growth Fin Structure

ABSTRACT

Boiling heat transfer associated with phase change is perhaps one of the most efficient cooling methodologies to manage extreme heat flux due to its large latent heat. Fin structures are used to further increase the magnitude of boiling heat transfer from the heated surface and have shown better performance than flat surface heat sinks. This work aims to experimentally investigate the heat transfer performance of two fin structures, namely regular and modified fins, in a pool boiling facility. The modified hollow fin structure is designed to enhance the regular fin's heat transfer performance by adding an artificial nucleation site. Heat transfer rates and heat transfer coefficients of the two fin structures are estimated in atmospheric pressure conditions using deionized water and compared with the literature. The results show that the regular fin heat sink shows a better heat transfer rate than the plane surface, while the modified fin structure shows higher heat transfer performance than the regular fin. This is attributed to the additional nucleation sites on the hollow fin, a better rewetting phenomenon, and therefore a favorable bubble growth and release mechanism. Also, a multilayer perceptron artificial neural network with a back-propagation training algorithm is applied for modeling the bubble departure diameter concerning wall superheat and subcooling level to predict the bubble behavior from the artificial nucleation site.

1. Introduction

The rapid advancement of nanotechnology and microelectronics has posed considerable challenges to the thermal management of extreme heat loads exceeding 1000 W/cm², discharged from tightly confined areas in many electromechanical systems. For example, in the processor Core i7-6700 K by Intel, the dissipated heat is rated at 95-110 W on the surface of a 13.52 \times 9.05 mm² (Menni et al., 2020, Zhou et al., 2022). To ensure a long lifetime and safe operation of microelectronic systems, we must maintain the operating temperature stable in its optimal condition by actively managing such high heat flux. Nucleate boiling heat transfer is probably one of the most efficient cooling methodologies for many systems due to a large amount of latent heat associated with the phase change (Ghazivini et al., 2021). The potential of innovative cooling systems associated with phase change has already provided considerable energy and cost savings in many thermal management applications (Hashemi et al., 2022, Hashemi and Jang, 2023, Fazel, 2010, Mikic and Rohsenow, 1969, Rini et al., 2002, Mourgues et al., 2013, Tang et al., 2019).

Research on the enhancement of boiling heat transfer has become a

hot topic as the heat dissipation demand has continuously increased (Zhou et al., 2022, Fan et al., 2015, Bertossi et al., 2015, Zhang and Kim, 2014). As a simple and economical approach, surface modification such as machining, surface deposition, and chemical corrosion can improve heat dissipation performance. The change of surface morphology has a significant impact on the bubble behavior during boiling, consequently on the heat transfer performance, which is different from that of the traditional smooth surface. To meet the heat dissipation requirement of high-power devices, numerous surface modification techniques have been considered, for example, micro-pin-finned structures. Wei and Honda (Honda and Wei, 2004, Honda and Takamatsu, 2003, Wei and Honda, 2003) conducted FC72 pool boiling experiments with different sizes of micro-pin-fins under various subcooling levels. Their boiling curves showed a sharp increase in the heat flux, and the critical heat flux (CHF) increase ratio is more than 300% of PF50-270 under 45 K subcooling. Chu et al., (Chu et al., 2012) also fabricated specific microstructure arrays to investigate the effect of roughness on pool boiling. The saturated water was used as the working fluid, and the most considerable CHF enhancement was ~160% on the roughest surface. Kim et al. (Kim et al., 2017) designed a set of pin-finned structures to

E-mail address: kimm@fau.edu (M. Kim).

^{*} Corresponding author

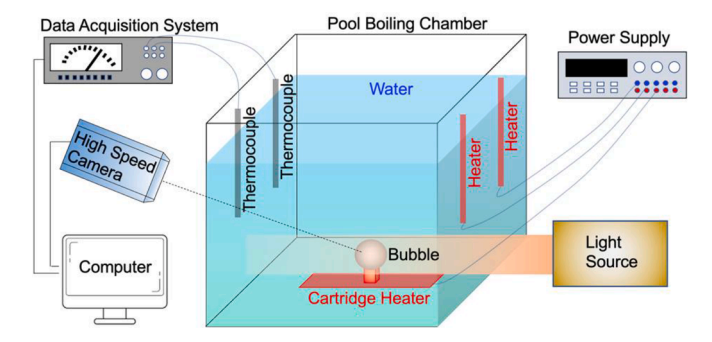


Fig. 1. Schematic diagram of the experimental setup.

study the effect of fin size on heat flux. The results showed an optimal gap size to achieve the best heat transfer performance, which is a 350% enhancement of CHF. Besides, Kim et al. (Honda and Takamatsu, 2003) also demonstrated an optimal channel width to reach the highest heat flux among different microchannel geometries with the same height. Xue et al. (Xue et al., 2013) experimentally studied nucleate pool boiling of FC-72 on the micro-pin-finned surface under microgravity in the heat fluxes of 7.2–27.2 W/cm² to enhance boiling heat transfer. Micro-pin-fins with the dimensions of 30 \times 60 μm^2 and the space of 30 µm were fabricated on the surface of square silicon with the dimensions of $10 \times 10 \times 0.5 \text{ mm}^3$ by using the dry etching technique. The micro-pin-finned chip showed a considerable heat transfer enhancement in the nucleate boiling region compared to a smooth surface under microgravity conditions. Walunj and Sathyabhama (Hamzekhani et al., 2015) fabricated the microchannels with rectangular, parabolic, and stepped geometries to investigate the effect of different shapes on bubble behaviors and heat transfer.

Even though pin-finned structures have been widely used in heat transfer enhancements, some modifications can be performed to further improve heat transfer performance. One advanced method is to artificially fabricate cavities on a surface (Markal et al., 2017, Markal et al., 2018, Zhang et al., 2021, Markal and Kul, 2022, Markal et al., 2022). These cavities serve as nucleation sites, and the quantity of cavities is one of the critical parameters to increase the heat transfer (Ghazivini et al., 2021). Not all the cavities generate bubbles, and, therefore, a minimum cavity radius exists at a specific heat flux so that the cavities greater than the minimum radius generate vapor bubbles, named active nucleation sites. The active nucleation site density is referred to as the number of cavities that form a vapor bubble per unit heating surface area. The active nucleation site density coupled with the bubble departure diameter is closely correlated with the boiling heat flux or the boiling heat transfer coefficient (Ghazivini et al., 2021).

The heat transfer enhancement of fin structures is induced by a change in bubble behaviors in nucleate boiling, which is a consequence of the surface morphology (Ghazvini et al., 2021). Since bubble behaviors in nucleate boiling significantly affect the heat dissipation from a heated surface, studying bubble behaviors with some key parameters such as bubble departure diameter, bubble departure frequency, and growth time require special attention. Many studies focused on understanding bubble behaviors to provide an acceptable physical mechanism and theoretical prediction. The process of bubble growth in the uniformly superheated liquid was analyzed by Bosnjakovic (Zhou et al., 2022) for the first time, who proposed that the continuous evaporation and growth of bubbles were maintained by the energy transferred from the superheated liquid to the bubble interface. Later, some researchers experimented on the bubble behavior on pin-finned surfaces in nucleate boiling (Markal et al., 2017, Markal et al., 2018). Zhang et al. (2021) experimentally investigated the nucleate boiling heat transfer of gas-saturated FC-72 on a micro-pin-finned surface with different dimensions. Experimental results showed that the bubble detachment radius increases with increasing heat flux, but the traditional force

balance model failed to predict the bubble detachment radius on micro-pin-finned surfaces, especially at high heat fluxes. Zhou et al. (2022) performed the pool boiling experiments on vertical surfaces under subcooled and near-saturated conditions. Using a high-speed camera with high temporal and spatial resolution, bubble behaviors on micro-pin-finned surfaces were observed. Different bubble growth modes on different surfaces were obtained, and the influence of the micro-pin-fins on the bubble growth and departure processes was learned. The results in the literature suggest that the bubble departure diameter and heat flux on pin-finned structures is more significant than on the smooth surface (Markal and Kul, 2022, Markal et al., 2022).

In this study, we introduce a new fin structure with an artificial nucleation site to further enhance the heat transfer performance of the heated surface during subcooled boiling. Subcooled boiling offers benefits such as increased heat transfer rates, prevention of critical heat flux, improved stability, enhanced bubble dynamics, reduced wall superheat, and achieving significant heat transfer enhancements at lower temperatures. We mainly investigate the heat flux and the bubble dynamics parameters of the new fin structure, such as bubble departure diameter, bubble departure frequency, and bubble growth time. The novelty of this study lies in integrating parabolic profile artificial nucleation site, occupying 0.25% of the fin volume, onto a fin structure. From our preliminary study, we found that this high volume of artificial nucleation site on top of the fin introduces a consistent generation of large bubbles, which provides a convenient visualization of transient bubble shape. The larger bubbles offer the finer resolution of temperature measurements, accurate differentiation of heat transfer mechanisms at the water-vapor interface. Thus, we focus on the heat transfer performance of two different fin structures, namely regular and modified fins, in a pool boiling facility, with a focus on the effect of an artificial nucleation site on heat transfer performance. While previous studies have employed solid fin structures to improve boiling heat transfer, this study specifically focuses on the use of an artificial nucleation site on the fin (i.e., a hollow fin) to enhance the performance of fin structures. The results are compared with those from a regular fin structure to understand the effect of the additional nucleation sites on heat transfer. Also, a multilayer perceptron (MLP) artificial neural network (ANN) with a back-propagation (BP) training algorithm is applied for modeling the bubble departure diameter with respect to wall superheat and subcooling level to predict the bubble behavior from the artificial nucleation site. This modeling approach would help understand bubble behaviors in nucleate boiling and consequently achieve a universal theoretical prediction of bubble growth in boiling. The mean square error (MSE) value of the model is calculated to evaluate the model's accuracy.

2. Materials and Methods

The experimental setup consists of a boiling chamber, test surfaces, data acquisition system, high-speed camera, light source, and heaters. DI water was used as a working fluid at atmospheric pressure, as shown in Fig. 1. The boiling chamber (120 \times 120 \times 120 mm³) made from transparent polymethylmethacrylate (PMMA, McMaster-Carr, Elmhurst, IL) sheets (6 \times 6 inch, 3.6 mm thick) was filled with 1 L DI water. The liquid temperature was measured by two K-type thermocouples (OMEGA Engineering) and controlled by two cartridge heaters (McMaster-Carr, 400W power, 2-inch length). The heater kept the working fluid at different subcooling levels from 25 K to near saturation temperature. A 50W LED dual gooseneck light source (AmScope, Irvine, CA) was utilized for the illumination, and the bubble phenomenon on the surfaces was captured by a high-speed camera (Fastec IL5, Fastec Imaging Corp., San Diego, CA) installed on a screw guide to precisely adjust its position. The high-speed camera recorded images of the boiling process at the maximum frequency of 100 frames per second. Also, Nikon AF micro-NIKKOR 60mm f/2.8D lens (B&H Photo Electronic Corp.) was mounted on the camera to achieve clear close-up images. The

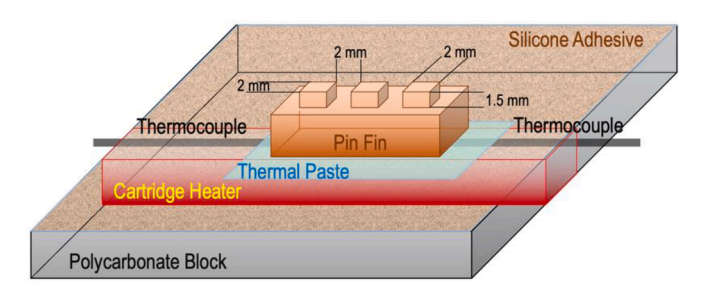


Fig. 2. Schematic of the test section.

Table 1Test conditions of the pool boiling experiments.

Test surfaces	Liquid subcooling levels (°C)	Pressure (atm)	Maximum effective heat flux (W/cm^2)
Regular fin surface Modified fin surface	20, 15, 10	1.0	32.26

images were then exported for processing, in which the segmentation and bubble behavior information extraction was completed using a MATLAB algorithm. The DC power supply connected through copper wires was used to control the heat flux of the surface and liquid temperatures. A layer of low thermal conductivity adhesive, which is a silicone sealant with a thermal conductivity of 0.18 W/(m·K), was applied on the non-structured area at the top side of the heated surfaces to ensure that only the fin area $(10\times4~\text{mm}^2)$ was the effective heat transfer surface. The wall temperature was measured by a K-type thermocouple pasted to the backside of the surface with a high thermal conductivity adhesive. The whole component was adhered to a polycarbonate base with a low thermal conductivity adhesive, as shown in Fig. 2. Table 1 presents the test conditions of the pool boiling.

The total heat flux provided by the DC power supply can be calculated as

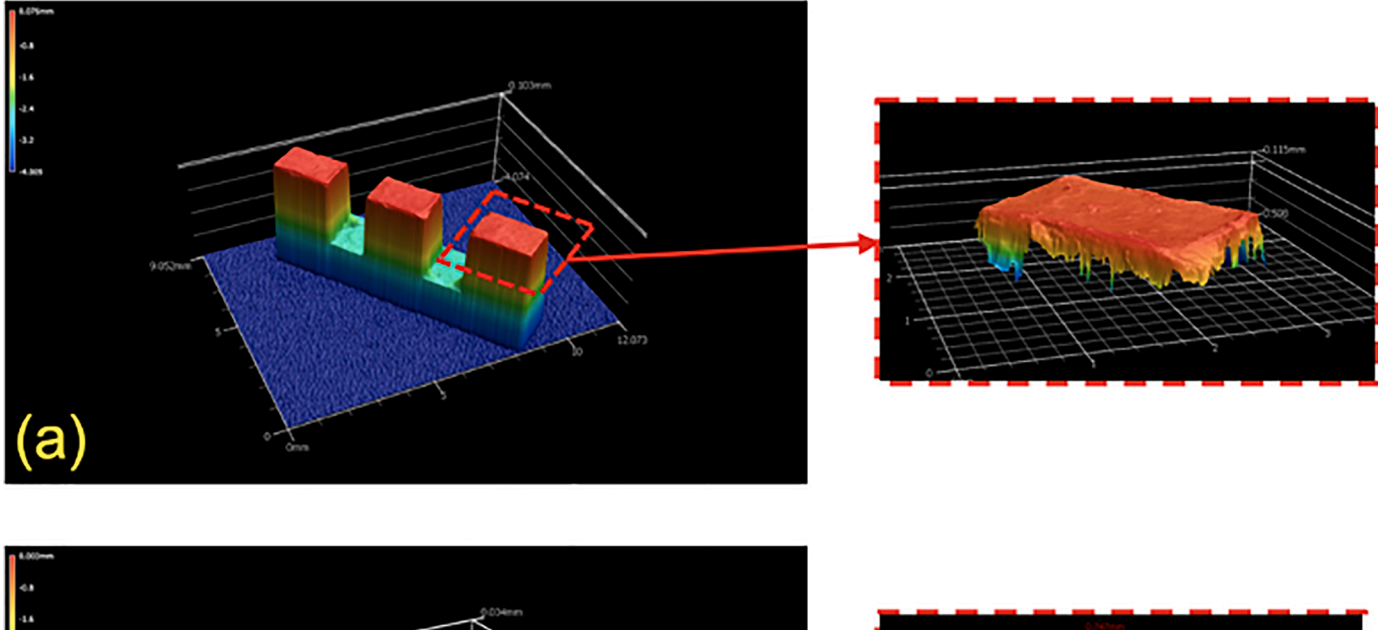
$$q_{total} = \frac{VI}{A} \tag{1}$$

where V and I are the voltage and current through the heated surface, and A is the effective heat transfer area. The wall superheat is,

$$\Delta T_{sat} = T_w - T_{sat} \tag{2}$$

where T_w and T_{sat} are the wall surface temperature and saturation temperature of the working fluid, respectively.

By knowing $q_{loss}=q_{total}-q_{e\!f\!f}$, the possible heat loss is calculated. Measuring the effective heat flux in a pin fin surface involves attaching thermocouples to the heat sink and measuring the temperature gradient between two different sections of the surface.



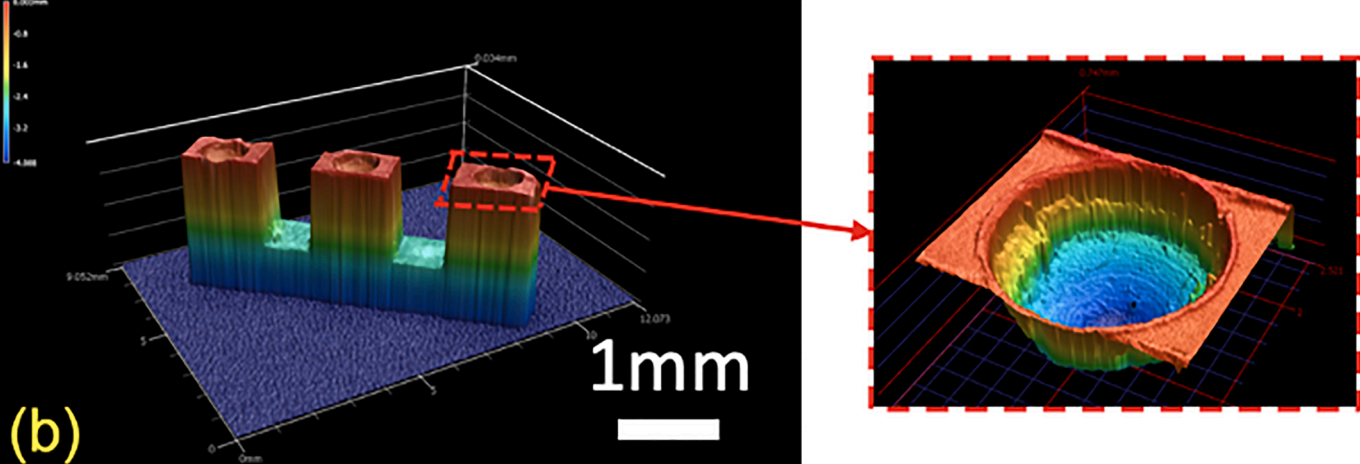


Fig. 3. 3D profiles of (a) the regular and (b) modified fin surfaces.

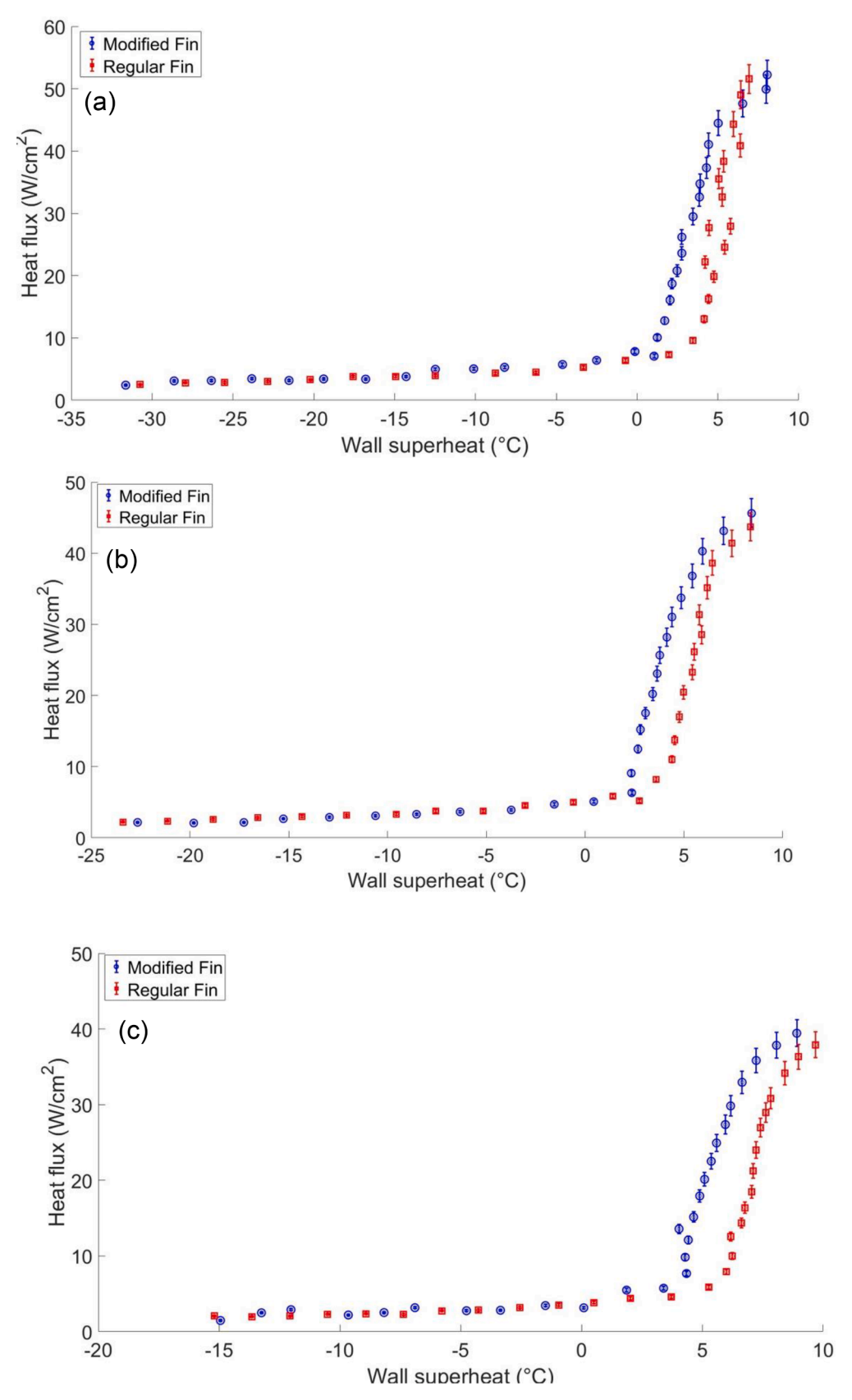


Fig. 4. Boiling curves of two different surfaces under various subcooling levels (a) 35 $^{\circ}$ C, b) 25 $^{\circ}$ C, and c) 15 $^{\circ}$ C).

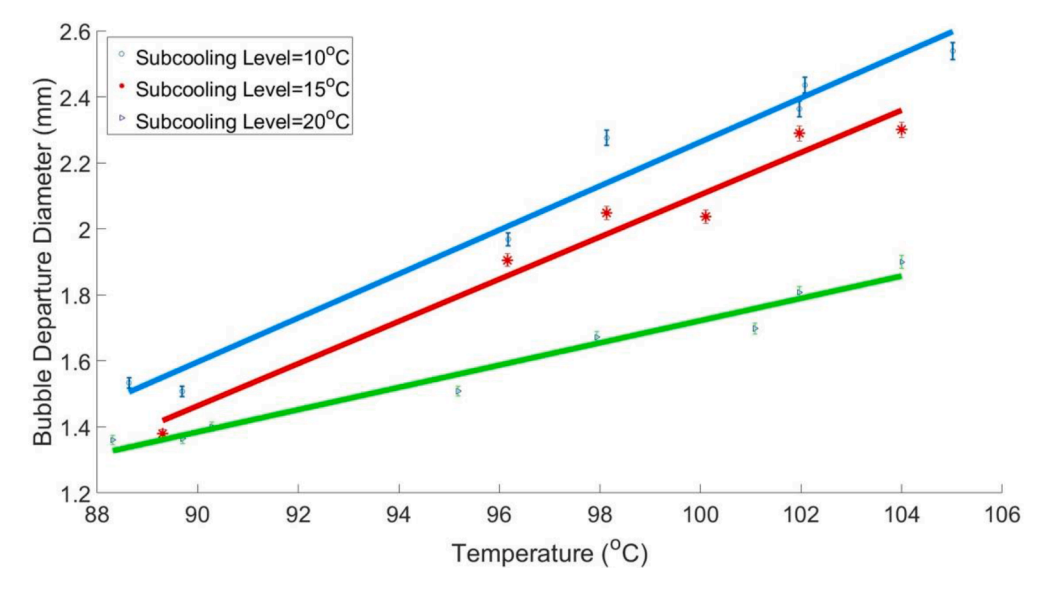


Fig. 5. Bubble departure diameter on the regular fin with respect to wall temperature at three different subcooling levels.

$$q_{eff} = k \frac{T_2 - T_1}{\Delta x} \tag{3}$$

where T_1 and T_2 are the temperatures measured by thermocouples in the upper and lower layers of the copper block. The distance separating two layers is denoted by Δx and has a value of 4 mm. The copper block used in the study has a thermal conductivity represented by k, which is equal to 380 W/(m·K). The maximum effective heat flux is 32.26 W/cm², and the heat equivalent heat loss is 1.69 W/cm², which is 5% of the total provided input.

The major uncertainty in the measured heat flux is through the temperature measurements and location data of the thermocouples. According to the error propagation theory (Mei et al., 2018), the uncertainty of the heat flux can be calculated using Eq. 4. The maximum uncertainty in the heat flux measurement is less than 4.5%. On the other hand, the wall temperature error is affected by various factors including thermocouple calibration error, temperature correction error, temperature fluctuation, and thermocouple resolution (0.5°C) . The total error in wall temperature measurement is estimated to be 0.55°C . Similarly, the bulk liquid temperature error of 0.54°C is composed of thermocouple calibration error (0.03°C) , temperature fluctuation (0.1°C) , and thermocouple resolution (0.5°C) . In addition to the factors mentioned earlier, it is important to acknowledge that there are other uncertainties present in the experiment that are challenging to measure precisely.

$$\frac{\delta q}{q} = \sqrt{\left(\frac{\delta k}{k}\right)^2 + \left(\frac{\delta \overline{\Delta T}}{\Delta T}\right)^2 + \left(\frac{\delta \Delta x}{\Delta x}\right)^2} \tag{4}$$

Six number of bubbles were obtained and averaged under the given input conditions. A high-speed camera was used to capture bubble images, which enable marking of four points on the bubble's top, bottom, left, and right. These points provide corresponding pixel coordinates that can be used to calculate the bubble diameter.

$$D = s(x_{right} - x_{right} + y_{up} - y_{down})/2$$
(5)

where s is the scale factor, representing the conversion of one pixel in the image to a distance. The bubble departure diameter was determined using the MATLAB function regionprops to extract the properties (x and y values) of the bubbles in the image. Next, thresholding and binarizing the image were implemented to convert the image into a binary format, where pixels belonging to the bubble region are assigned a value of 1 (foreground), and the remaining pixels representing the background are assigned a value of 0. After thresholding and binarizing the image,

regionprops can be used to calculate the diameter of each detected bubble.

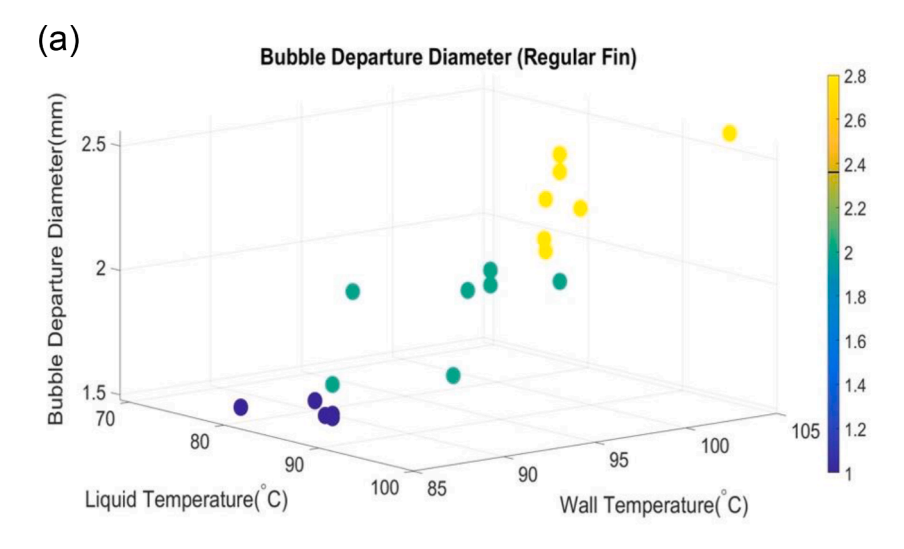
The parabolic artificial nucleation site was created by mechanical indentation at the center of the fin structure, which is 500 μm deep in diameter of 300 μm on the top surface (Fig. 3). A 3D optical profilometer (Keyence VR-6000) was used to perform non-contact surface and roughness measurements. This 3D profile system captures full surface data across the target with a resolution of 0.1 μm , enabling measurement of features that cannot be performed with probe-type instruments. Fig. 3 shows the 3D profiles of the regular and modified fin surfaces, in which diameter of the artificial nucleation site is approximately 300 μm .

3. Results and discussion

3.1. Heat transfer performance of fins in pool boiling

Pool boiling curves relating to the heat flux and wall superheat (Eq. 2) are used to characterize the heat transfer performance of the tested surfaces. Fig. 4 shows the boiling curves for the two different surfaces under three liquid subcooling levels. In all subcooling levels, the surface with an artificial nucleation site shows lower wall temperature at the same heat flux or higher heat flux at a given temperature. It can be found that in the convection boiling region at a temperature range from 70 to $100\,^{\circ}$ C (i.e., $\Delta T_{sat} = -30 \sim 0\,^{\circ}$ C), there is no significant difference in heat flux between the surfaces. On the other hand, the heat transfer performance of the modified fin is better than the regular fin when the nucleate boiling region begins ($105 \sim 115\,^{\circ}$ C). The boiling curve of the modified fin is shifted to the left of the curves of the regular fin, and the wall temperature of the modified fin is $2-4\,^{\circ}$ C lower than that of the regular fin at the same heat flux.

When comparing with a fin without an artificial nucleation site, the presence of the artificial nucleation site can result in lower wall temperatures at the same heat flux. This phenomenon can be attributed to enhanced boiling heat transfer characteristics and the ability to promote more efficient cooling. The presence of artificial nucleation sites in a fin enhances boiling heat transfer in multiple ways. These sites, which can be surface irregularities or cavities, serve as preferential locations for bubble formation, promoting more efficient heat transfer from the heated surface to the liquid. Additionally, the nucleation sites increase the active boiling area, creating additional pathways for heat transfer. This enlarged surface area facilitates enhanced cooling compared to a fin without nucleation sites. Furthermore, the nucleation sites aid in liquid replenishment by generating convective currents as bubbles form and



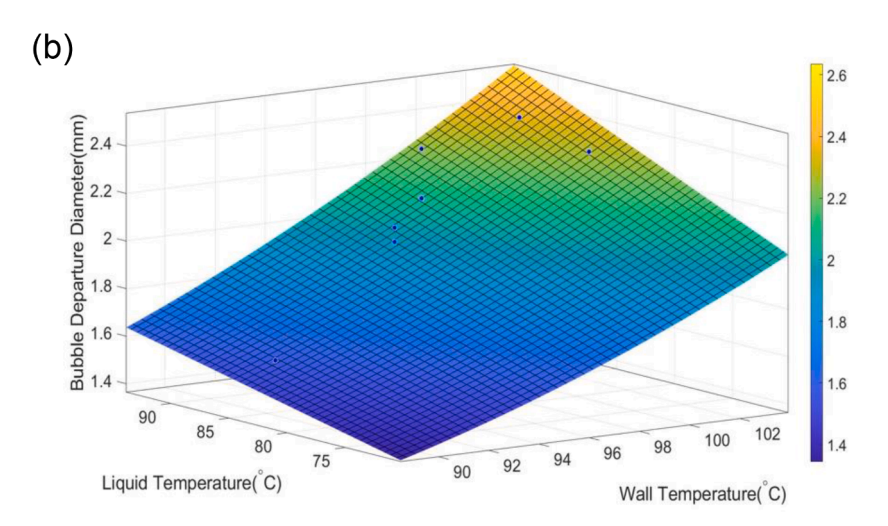
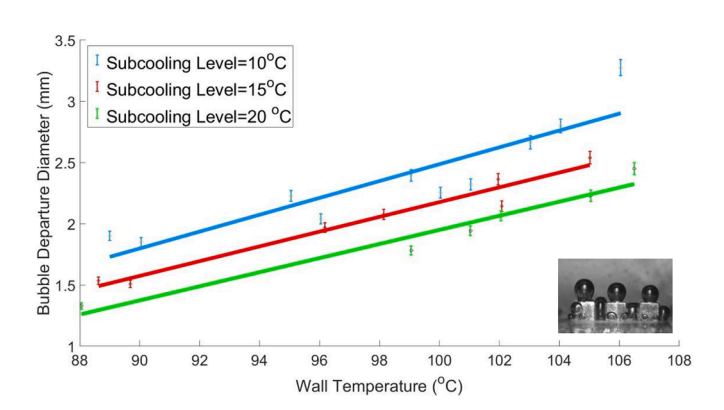


Fig. 6. a) 3D scattered and b) fitted surface plots for the bubble departure diameter on the regular fin.



 $\begin{tabular}{ll} Fig.~7. Bubble departure diameter on the modified fin with respect to wall temperature at three different subcooling levels. \\ \end{tabular}$

detach, promoting the transport of cooler liquid towards the heated surface. This replenishment process helps cool the boundary layer and ultimately reduces the temperature at the wall.

3.2. Bubble departure diameter

To investigate the bubble behavior in nucleate boiling on the two fin

structures under different conditions, the experiments were conducted at different subcooling levels of 10 °C, 15 °C, and 20 °C. Because the violent bubble interaction at high heat fluxes impedes accurate observation of the bubble behavior, all the experiments were carried out under a heat flux of less than 4 W/mm 2 , ensuring continuous single bubble generation.

Our particular interest is in the investigation of the bubble departure diameter (D_d) that explains the effects of wall temperature and subcooling level on the heat transfer performance, and it has been one of the vital parameters in determining the nucleate boiling heat transfer coefficient (Ghazivini et al., 2021). The bubble departure diameter is also a critical parameter that determines heat transfer coefficients using various empirical or semi-empirical correlations (Ghazivini et al., 2021). It is generally understood that the bubble departure diameter is the ultimate or equal diameter of the vapor bubble once it detaches from the heated surface during the boiling (Ghazivini et al., 2021). We determine the bubble departure diameter based on images or videos of transient vapor bubbles taken by a high-speed camera. Image processing software is then used to evaluate the equivalent diameter of the vapor bubble. Fig. 5 shows the effect of wall temperature and subcooling levels on the bubble departure diameter for the regular fin. The diameter increases by increasing wall temperature and subcooling levels-it is approximately 2.56 mm for wall temperature at 106 $^{\circ}$ C and subcooling level at 10 $^{\circ}$ C. Fig. 6 shows 3D scattered and fitted surface plots for the bubble departure diameter in the regular fin. In Fig 5 and 6, one interesting

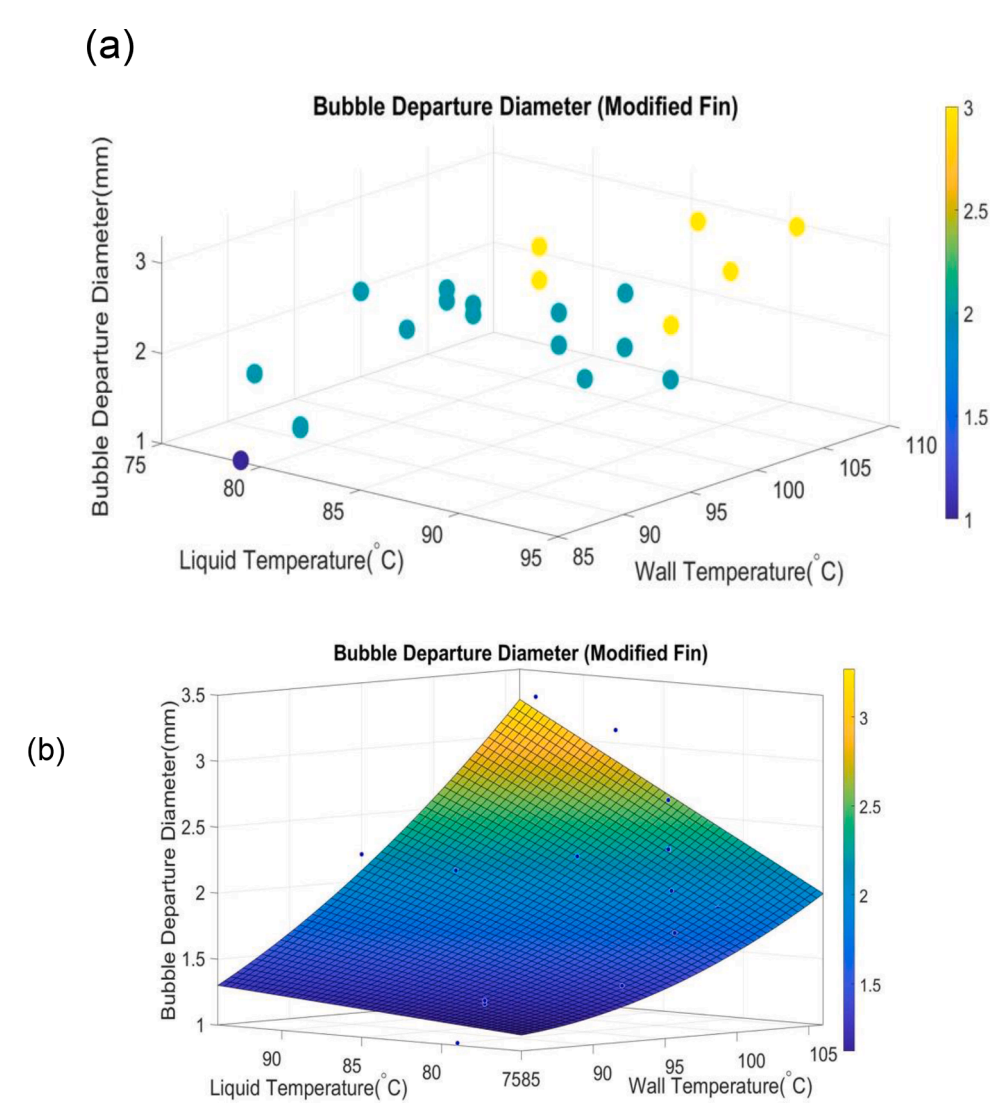


Fig. 8. a) 3D scattered and b) fitted surface plots for the bubble departure diameter on the modified fin.

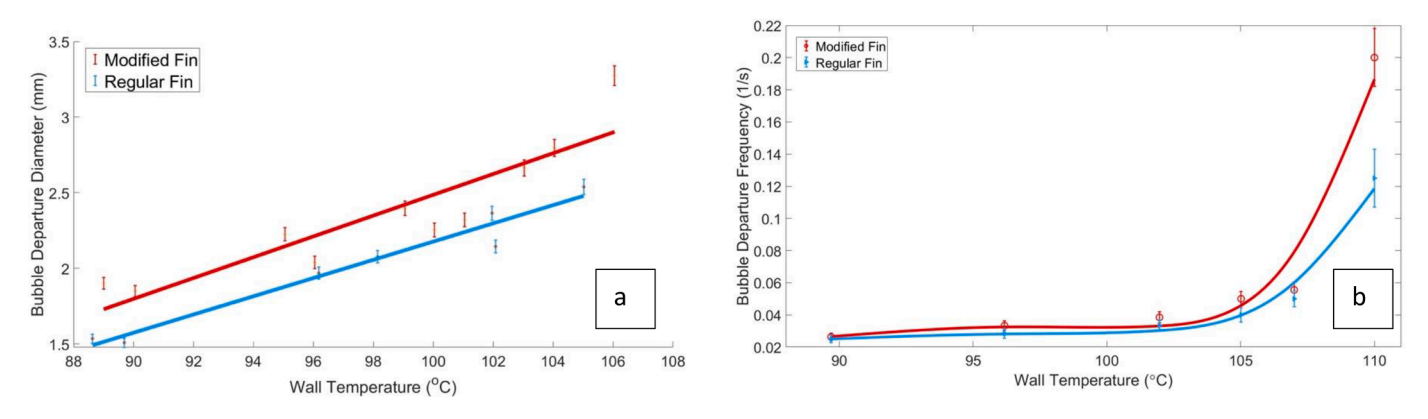


Fig. 9. a) Bubble departure diameter and b) bubble departure frequency of both surfaces at subcooling level of 10 °C.

observation is that the bubble departure diameter increases linearly with wall temperature when decreasing the subcooling level. On the other hand, the effects of wall temperature on the bubble departure diameter at different subcooling levels in the modified fin are presented in Figs. 7 and 8. It can be seen that, like the regular fin, the bubble departure diameter increases by increasing the wall temperature and reducing the subcooling level, showing approximately 3.3 mm at a wall temperature

of 106 $^{\circ}$ C and a subcooling level of 10 $^{\circ}$ C. Based on our observation, the onset of nucleate boiling happens at wall superheat= 2 $^{\circ}$ C and subcooling level= 30 $^{\circ}$ C. Through the use of artificial nucleation sites, it is possible to achieve ONB at relatively low wall superheats, sometimes even below 1 $^{\circ}$ C. This is because the presence of nucleation sites provides favorable locations for the formation of vapor bubbles, reducing the energy barrier required for bubble nucleation. Consequently, the boiling

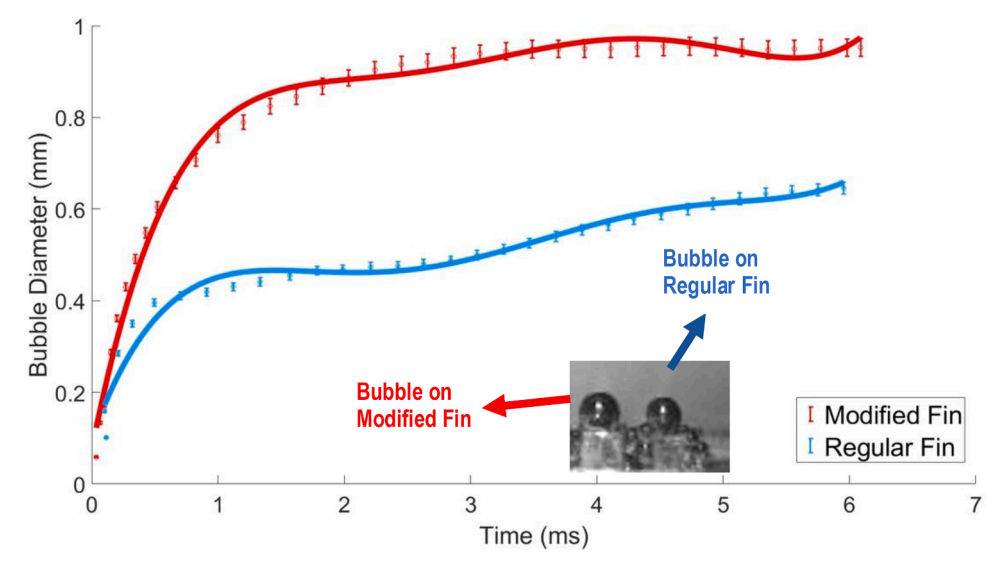


Fig. 10. Bubble growth curves for different surfaces at wall temperature of 105 $^{\circ}$ C and subcooling level of 10 $^{\circ}$ C.

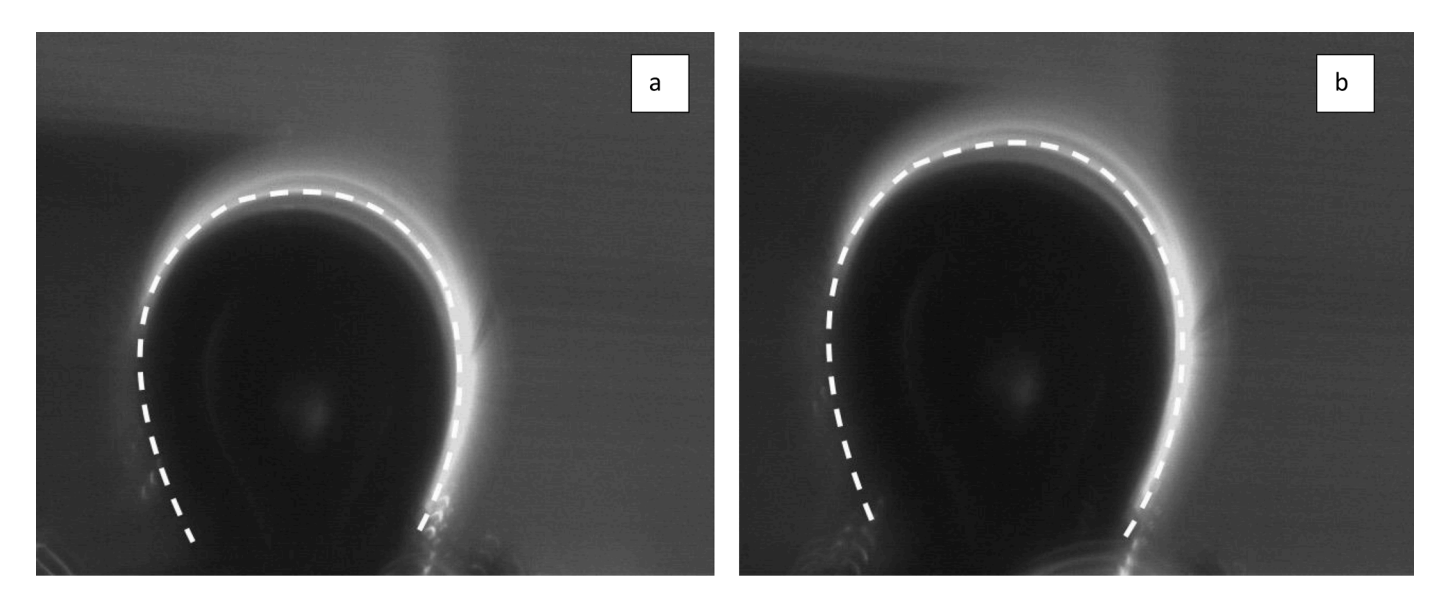


Fig. 11. Bubble growth on a) regular fin, b) modified fin at the same time at wall temperature of 105 °C and subcooling level of 10 °C.

process can initiate at lower superheats, resulting in an earlier ONB.

3.3. Comparison between regular and modified fins

To better understand the effect of an artificial nucleation site on the fin, the bubble departure diameter, bubble departure frequency, and bubble growth time in the regular and modified fins are compared at a wall temperature of 105 °C and a subcooling level of 10 °C, as shown in Fig 9 and 10. In Fig. 9a, although the data for the bubble diameter seem scattered along the wall temperature, the size of the departure diameter increases with increasing the wall temperature. Also, the bubble departure diameter for the modified fin is considerably higher than that of the regular fin at a given time and wall temperature. This is most likely because the artificial nucleation site on top of the modified fin facilitates bubble initiation and growth due to an increase in the boiling surface area. Particularly, the difference in the departure diameter between the modified and regular fins is much larger when the wall temperature is above 100 °C than when it is less than 100 °C. Also, Fig. 9b shows the bubble departure frequency on the modified and regular fin surfaces. According to Fig. 9b, higher bubble departure frequency can be achieved on the modified fin compared to the regular fin at a given wall temperature (approximately 20% higher at low wall temperatures, $T_{wall} < 105^{\circ}C$), and 35% higher at high wall temperatures, $T_{wall} > 105^{\circ}C$). The sudden increase in bubble departure frequency with increasing wall temperature is attributed to the higher vaporization rate and thermal energy transfer at elevated temperatures, leading to more rapid formation and detachment of bubbles from the heated surface (Hamzekhani et al., 2015).

The bubble growth rate is the variations of bubble diameter with time, which is another significant parameter contributing to the boiling heat transfer coefficient. Fig. 10 shows the changes in bubble diameter from its initiation to departure along with time, which indicates the bubble growth time. In this figure, the bubble diameter increases dramatically in the early stage of the bubble growth (< 0.5 ms) due to the nucleation of the bubble on the artificial nucleation site, called the inertia-controlled phase of bubble growth. During this stage, there is an approximately linear relationship between the bubble diameter and time. At > 0.5 ms, the initiated bubble grows up at a slower rate compared to the initial stage and keeps a stable growth for a longer time (> 3 ms). In Fig. 10, at the end stage of the bubble growth, the bubble

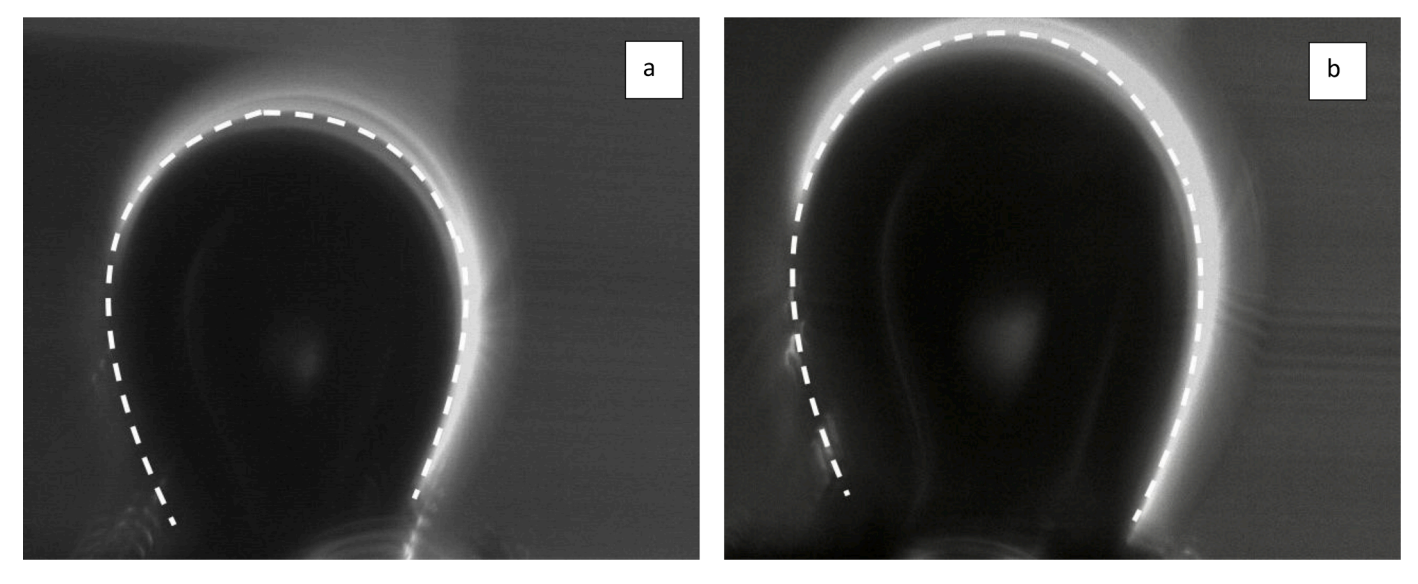


Fig. 12. Bubble departure on a) regular fin, b) modified fin at the same time at wall temperature of 105 $^{\circ}$ C and subcooling level of 10 $^{\circ}$ C.

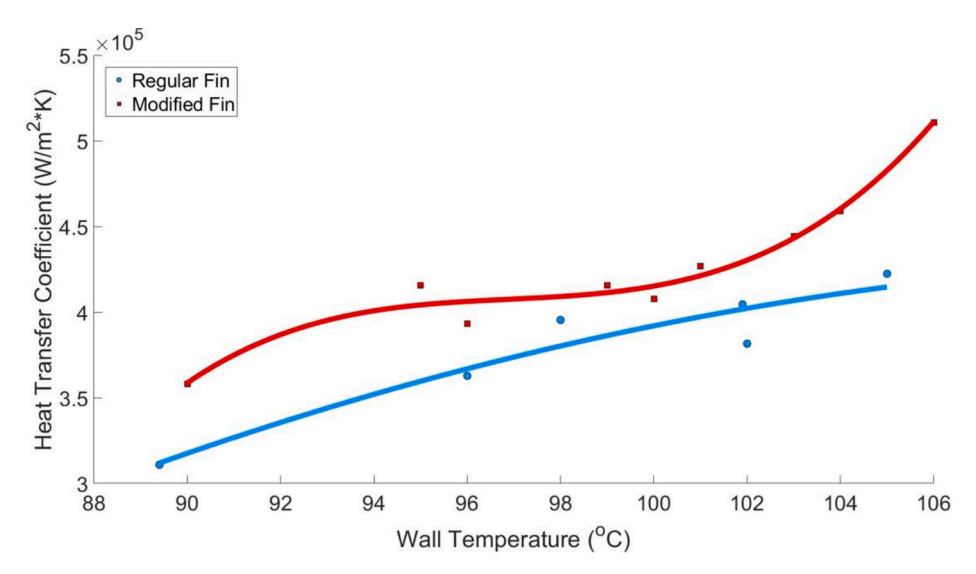


Fig. 13. Heat transfer coefficient of the regular and modified fins using Rohsenow correlation.

Table 2Traditional models for the prediction of the bubble growth curve.

Ref.	Author	Correlations
(Cole and Shulman, 1966)	Cole and Shulman	$D=5 Ja^{0.75}\sqrt{\alpha_l t}$
(Mikic et al., 1970)	Mikic	$R^+ = \frac{2}{3}[(t^+ + 1)^{1.5} - (t^+)^{1.5} - 1]$
		$R^+ = \frac{R}{B^2/A}, t^+ = \frac{t}{B^2/A^2},$
		$A = \left[b rac{\Delta T h_{fg} ho_{v}}{T_{sat} ho_{l}} ight]^{1/2}, B =$
		$\left[rac{12}{\pi}Ja^2lpha_l ight]^{1/2}$
(Forster and Zuber, 1954)	Foster and Zuber	$D=3.544Ja\sqrt{a_lt}$

leaves the nucleation site under the buoyancy force with its largest diameter (3.33 mm for the modified fin vs. 2.56 mm for the regular fin). The results in Fig. 9 and 10 suggest that the bubble initiation, growth, and departure from the modified fin take place at a faster rate than those of the regular fin. The fast ebullition cycle of the bubble leads to bubble

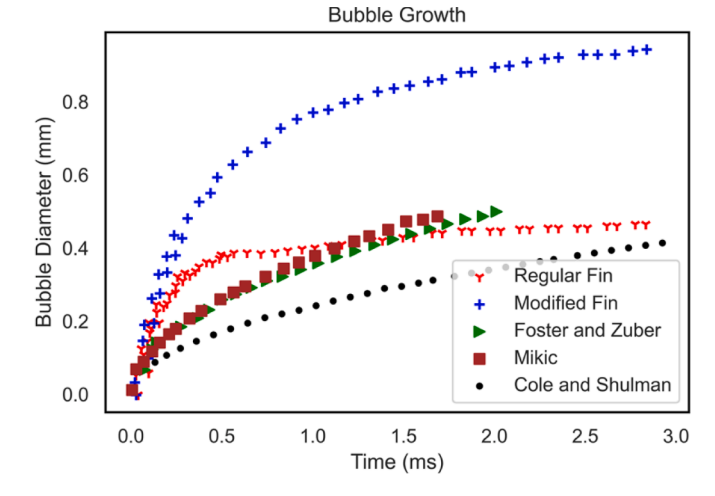


Fig. 14. The comparison of the bubble growth models, including the traditional models and the experimental data of the current study for the two different fin structures.

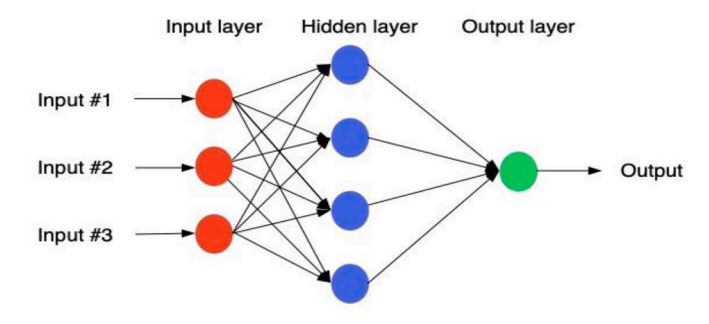


Fig. 15. Example schematic of a neural network structure

Table 3Inputs and the number of samples for each output parameter.

Output	Inputs		Number of samples
Bubble departure diameter (mm)	Wall temperature (°C)	Subcooling level (°C)	138

generation at a higher frequency. For the surface with a high bubble frequency, the local wall temperature would be lower because the rapid bubble nucleation takes away large amounts of heat from the heated surface. Fig. 11 and 12 show bubble shapes during growth time and departure time on the regular and modified fins.

In the present study, we utilized the Rohsenow correlation to estimate the heat transfer coefficient, which is known to offer a reliable approach for estimating the heat transfer coefficient based on the bubble departure diameter (Pioro, 1999). In the Rohsenow correlation, the liquid density, gravity acceleration, and wall superheat, and the latent heat of vaporization are needed. All considered values are related to water at atmospheric pressure including $\rho_l = 1000 \frac{kg}{m^3}$ and $h_{fg} = 2260000 \frac{J}{kg}$.

$$h = C \left(\rho_l \times h_{fg}^2 \times g \right)^{0.5} (\Delta T_w)^{0.5} \times d_b^{0.67}$$
 (6)

where C, ρ_l , g, ΔT_w are an empirical constant, the liquid density, gravity acceleration, and wall superheat. Also, h_{fg} and d_b represent the latent heat of vaporization and bubble departure diameter.

Our study reveals compelling evidence that the modifications made to the fin design have yielded substantial improvements in heat transfer performance when compared to the regular fins (Fig. 13). The enhanced heat transfer coefficients achieved with the modified fins clearly indicate a more efficient transfer of thermal energy from the fin surface to the working fluid. This, in turn, has the potential to greatly enhance the cooling effectiveness of the system. Specifically, our results demonstrate that the heat transfer coefficient for the modified fin is approximately 20% higher than that of the regular fin. This noteworthy increase in heat transfer efficiency is a testament to the effectiveness of the modifications made to the fin design.

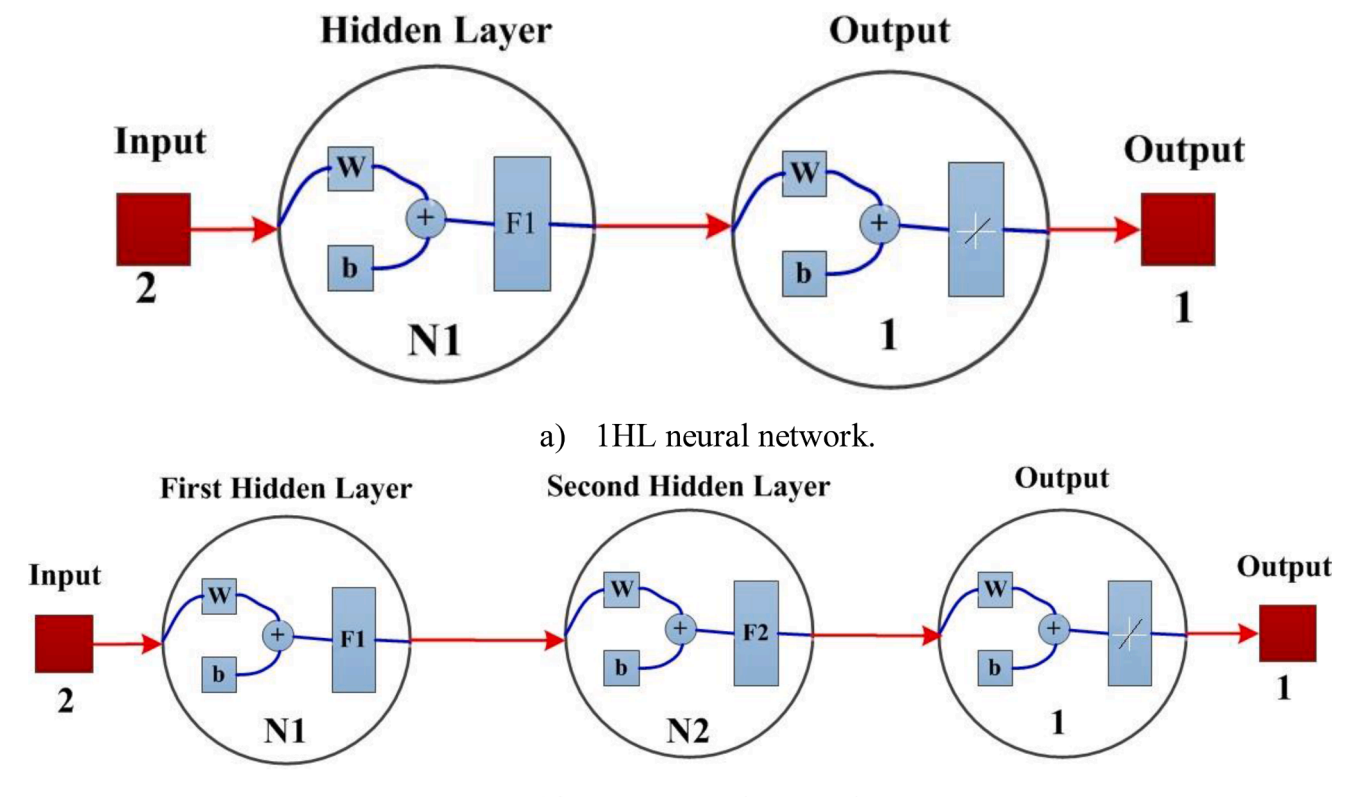
The characteristics of the bubble behavior can affect the heat transfer coefficient, which is a measure of the rate of heat transfer from the surface to the surrounding fluid. The heat transfer coefficient is influenced by the size, shape, and frequency of the bubbles formed on the heating surface. The larger the bubble departure diameter, the higher the heat transfer coefficient (Ghazivini et al., 2021). The shorter the bubble growth time and the higher the bubble departure frequency, the higher the heat transfer coefficient. One efficient approach to enhance bubble growth and heat transfer coefficient is to utilize artificial nucleation sites. Having an artificial nucleation site in nucleate boiling can lead to a higher heat transfer rate due to several factors. First, the addition of an artificial nucleation site provides a preferential location

for bubble formation, which can lead to more uniform and controlled bubble growth (Markal and Kul, 2022). This can increase the contact area on the heated surface available for heat transfer and promote more efficient heat transfer from the heated surface. Secondly, the presence of an artificial nucleation site can improve the rewetting behavior of the surface, promoting more stable and efficient heat transfer by preventing the formation of dry spots on the surface and enhancing the heat transfer coefficient. When a surface becomes dry or develops dry spots during heat transfer processes, it can hinder the efficient transfer of heat (Yajima et al., 2022). Dry spots act as thermal barriers, reducing the contact area between the surface and the liquid, and impeding the heat transfer process. This can lead to localized overheating and potential damage to the system. Additionally, the presence of an artificial nucleation site can lead to a lower wall superheat, which is the difference between the wall temperature and the saturation temperature of the liquid. This reduction in wall superheat is primarily due to the enhanced bubble formation and nucleation characteristics provided by the artificial nucleation site (Yajima et al., 2022). A lower wall superheat can lead to more efficient heat transfer as it reduces the thermal resistance at the heated surface. The artificial nucleation site can also lead to larger bubble departure diameters, which refer to the size of the bubbles as they detach from the heated surface. Larger bubble departure diameters along with faster bubble growth leads to a more efficient heat transfer process. The following correlations have been provided to mathematically understand the effect of the bubble behavior and nucleation site on the heat transfer coefficient.

In conclusion, the inclusion of artificial nucleation sites in nucleate boiling offers significant advantages in terms of improving heat transfer efficiency. These sites reduce the wall superheat, promote larger bubble departure diameters, and enhance bubble growth, all of which contribute to more efficient heat transfer processes. By optimizing the design and utilization of artificial nucleation sites, researchers and engineers can unlock the full potential of nucleate boiling and achieve enhanced thermal performance in various applications ranging from electronics cooling to power generation.

3.4. The bubble growth model

Over the past decades, many mathematical models have been proposed to describe the bubble growth process from the perspective of heat transfer and energy conversion. One of the classical models is the bubble growth in the homogeneous superheated liquid proposed by Bosnjakovic and Jakob (Zhou et al., 2022), $\frac{dR}{dt} = \frac{k}{h_{lr}\rho_r} \frac{(T_o - T_s)}{\sqrt{\pi \alpha_t t}}$, where k is the liquid thermal conductivity, h_{lv} is the latent heat, ρ_v is the vapor density, T_0 - T_s is the liquid superheat, and α_l is the liquid thermal diffusivity. Because of the ideal conditions for this model, various modifications are needed for the actual process under different conditions, and a variety of improved models have been produced on this basis, as shown in Table 2. Fig. 14 shows the bubble growth models developed by the traditional models while comparing the experimental data of the current study for the two different fin surfaces. It shows that the results of Mikic (Mikic et al., 1970) and Forster & Zuber (Forster and Zuber, 1954) models are in relatively good agreement with the bubble diameter on the regular fin surface at the initial stage, although the growth rate of traditional models is much smaller than the experimental result. This is because the traditional models were established based on a smooth surface while the heat transfer from the fins was not considered. On the other hand, none of the traditional models predict bubble growth on the modified fin surface. Besides, the bubble diameter from traditional models continuously increased with time. The initial growth rate of traditional models is much smaller than the experimental result of the modified fin, mainly because traditional models are established based on smooth surfaces. In the bubble formation on the modified fin which has an artificial nucleation site, despite relatively bigger vapor bubbles, the nucleation actively continues, and the sustainability of available bubbles continues



b) 2HL neural network.

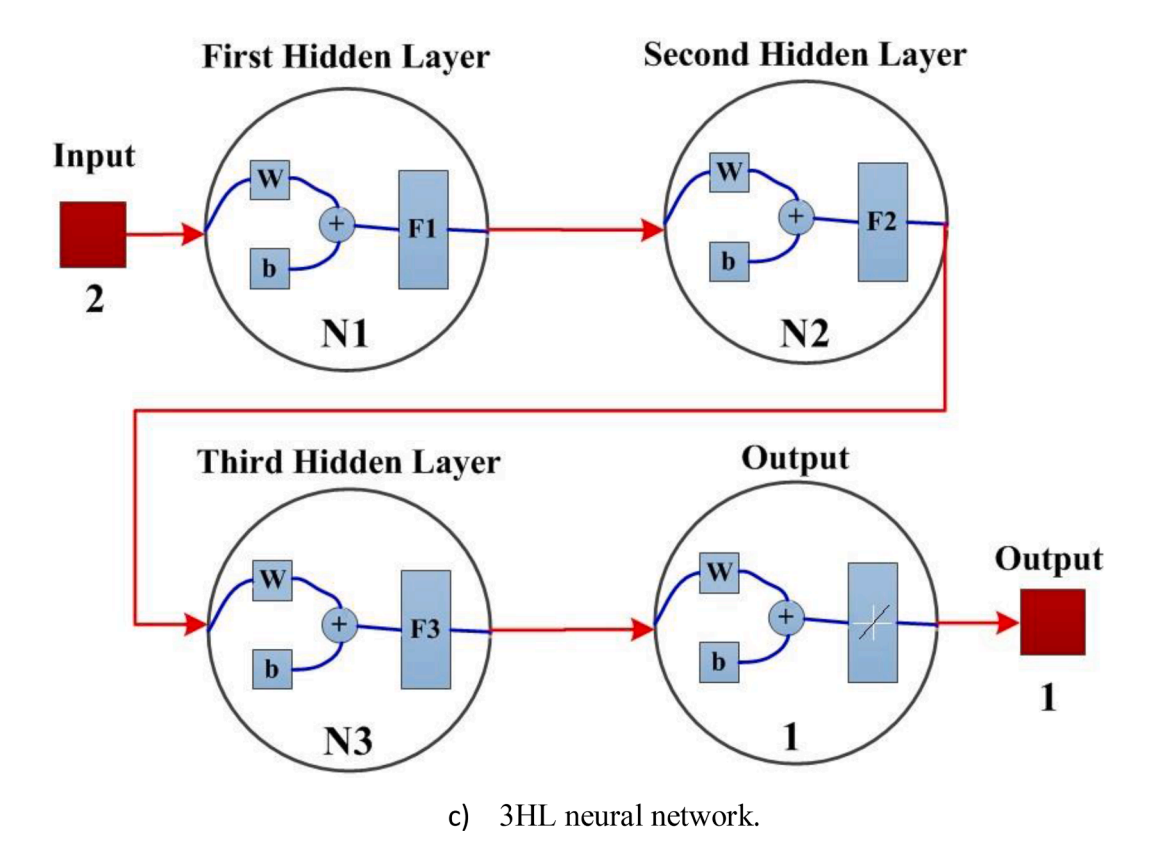


Fig. 16. A typical structure of the neural network with different hidden layers.

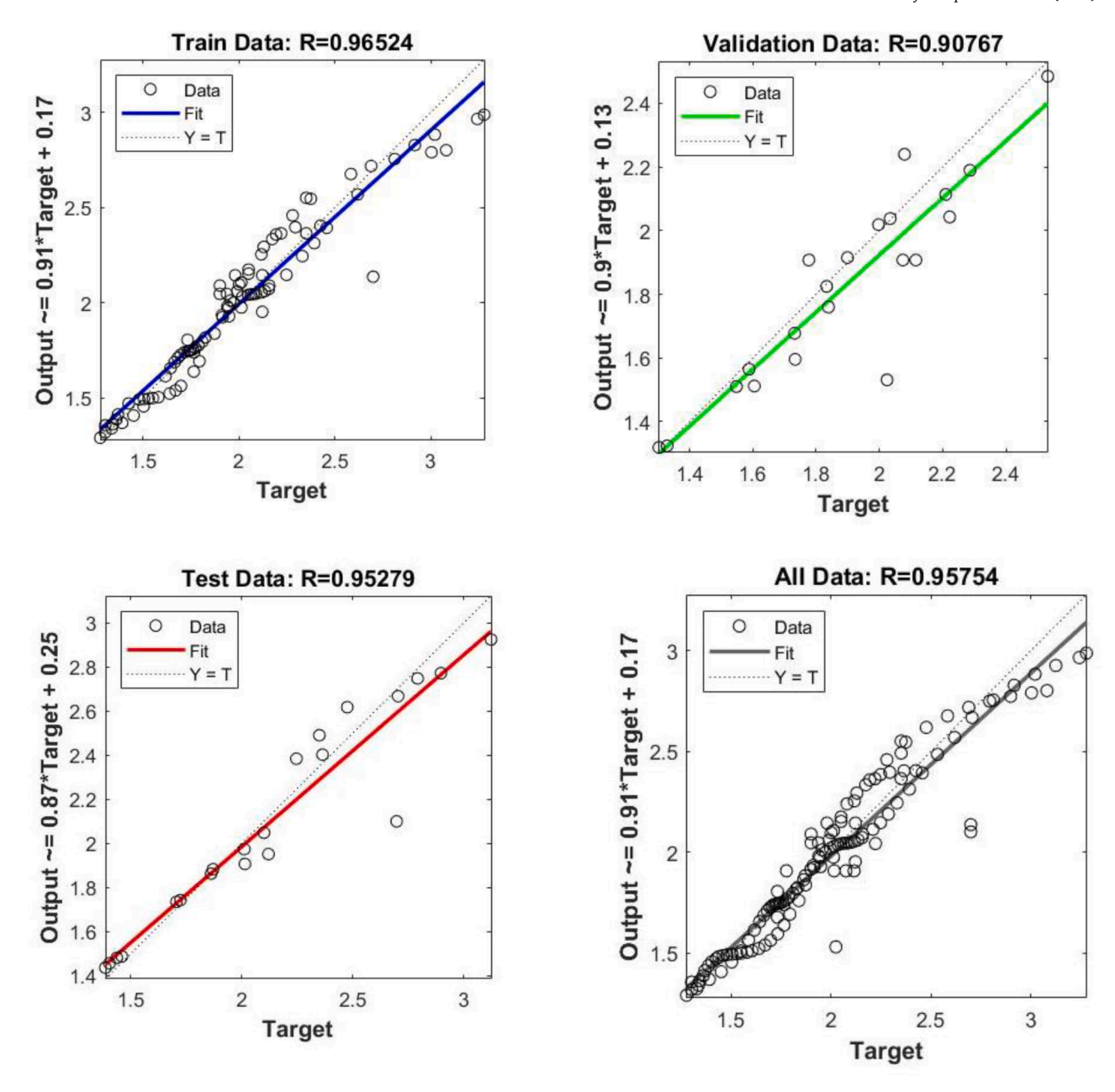


Fig. 17. Regression diagrams of the MLP network for bubble departure diameter with the 1HL network.

without any suppression. This phenomenon leads to a higher heat transfer coefficient and lower wall temperature.

3.5. Modeling of bubble departure diameter by MLP network

Conducting two-phase experiments or full CFD simulations often requires a high cost and time commitment. Bubble dynamics parameters like bubble departure diameter in nucleate boiling are usually a function of many independent variables, including liquid and wall temperatures, each valid over a finite range of values. The relationship between these parameters and their relevance can be deduced using new computing techniques. A promising technique that can be applied is the use of soft computing. In the past three decades, unprecedented development of soft computing techniques has been seen, such as Artificial Neural Networks (ANNs), Genetic Algorithms (GA), Genetic Programming (GP), Fuzzy-logic Control, and Data Mining, and their application in many scientific and engineering practices. Out of these, ANNs, which are inspired by the biological nervous systems of humans, learn to perform

tasks by utilizing available data without the need for programmed task-specific rules (Qiu et al., 2020). An artificial neural network (ANN) is a major modeling technique of data in different engineering problems, including heat transfer and boiling phenomena (Ghazvini et al., 2020). It is an information-processing machine developed based on the operation of the brain's neural network. The network's processing units are neurons connected through communication links, each with an associated weight. A standard neural network has considerable amounts of neurons and their connections (Ertuğrul, 2018). The fundamental elements of an ANN are a network architecture, learning algorithm, and transfer function, and changing these elements makes ANN methods distinct from other artificial neural networks.

In the current study, a multilayer perceptron (MLP) neural network with a back-propagation (BP) training algorithm is utilized to optimize the ANN-based modeling. In the BP training algorithm, the weights of the neuron connections are adjusted based on the discrepancy between the desired network outputs and the predicted outputs (Herzog et al., 2020). An MLP network composes of one input layer, one output layer,

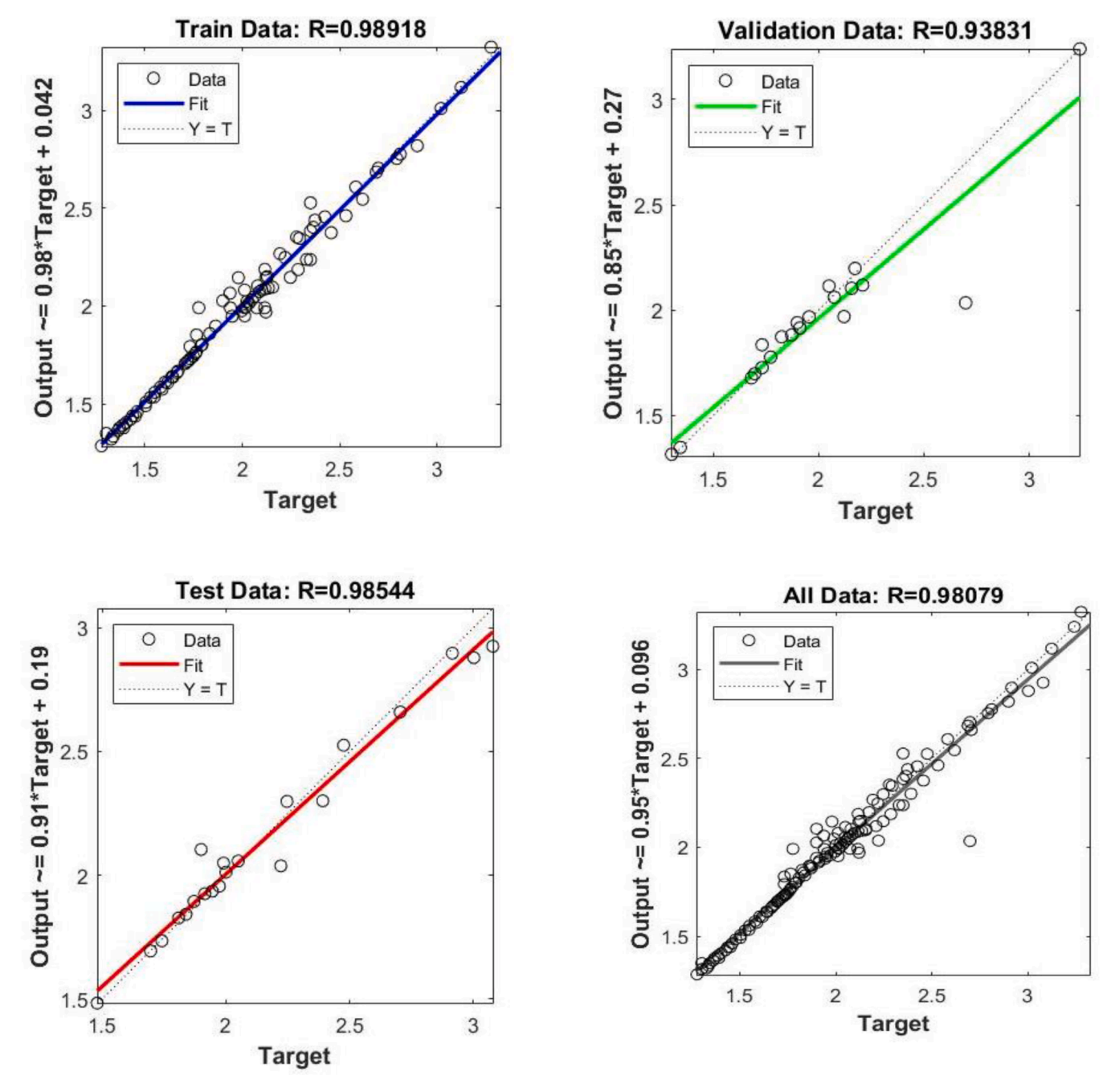


Fig. 18. Regression diagrams of the MLP network for bubble departure diameter with the 2HL network.

and one or more hidden layers (Fig. 15). The number of neurons in the input and output layers relies upon the number of input and output parameters of the problem, whereas the number of hidden layers and the neurons in each hidden layer can be selected by the designer's choice. Moreover, the transfer function of the neurons in the hidden and output layers can be chosen by the designer. Thus, the performance of this method is susceptible to these selectable parameters, and, in particular, the results are sensitive to the number of neurons in each hidden layer and the transfer function in each layer. The network's architecture can be optimized to produce the minimum error for the best performance. In this way, the network's performance is determined based on the MSE values between the desired output and the predicted output from the networks.

To model the bubble departure diameter with the neural network, the obtained experimental dataset is divided randomly such that 70% of

the dataset is utilized for training, 15% for testing, and the last 15% for validation. To train the network, the Levenberg-Marquardt algorithm is applied because it is commonly used and very robust in mathematics and computing, which means that in many cases Levenberg-Marquardt algorithm finds the best solution even if it starts very far off the final solution (Sayed et al., 2014). The input variables and the number of samples for each case are presented in Table 3. All datasets are normalized before being applied to the neural network. Normalizing the data generally speeds up learning and leads to faster convergence. Fig. 16 shows the typical structure of the 1HL, 2HL, and 3HL networks applied in this study, where *W, b*, and *N1* represent the weight, bias, and number of neurons for the neural network.

In the proposed neural network-based modeling approach, the input parameters are the wall superheat and subcooling levels, while the output parameter is the bubble departure diameter from the modified fin

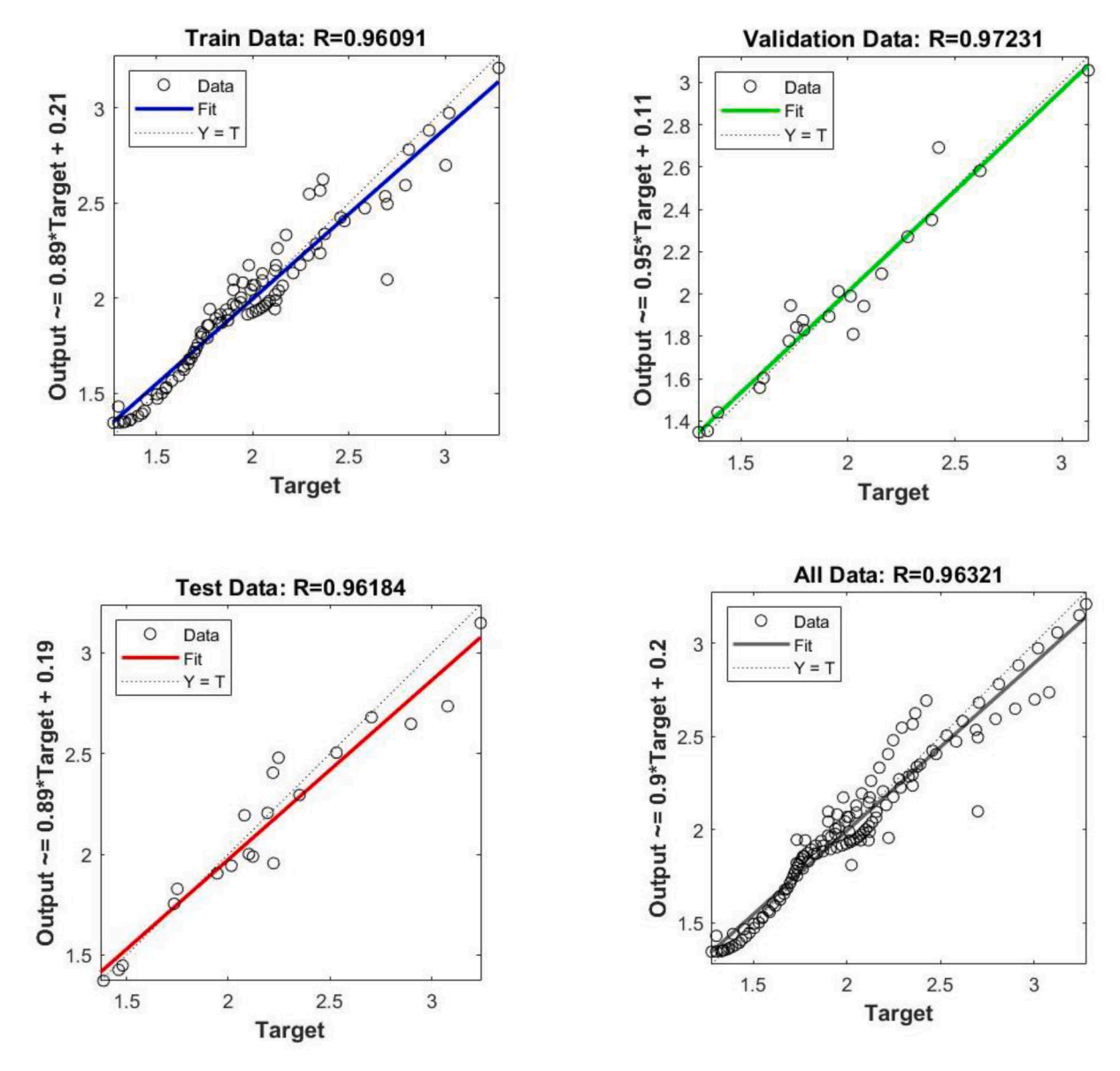


Fig. 19. Regression diagrams of the MLP network for bubble departure diameter with the 3HL network.

surface. These input parameters are critical factors that affect the bubble dynamics and heat transfer performance in nucleate boiling. The wall superheat represents the temperature difference between the heating surface and the bulk fluid, while the subcooling level indicates the degree to which the bulk fluid temperature is below its saturation temperature. By incorporating these parameters as inputs to the neural network, the model can effectively capture the complex interplay between the fluid flow, heat transfer, and bubble dynamics in nucleate boiling and accurately predict the bubble departure diameter from the modified fin surface.

Figs. 17-19 show the regression diagrams for the best MLP network with 1HL, 2HL, and 3HL networks for bubble departure diameter, respectively based on the specifications in Table 3. In these diagrams, the MLP network with one hidden layer can approximate the desired outputs based on the values of the correlation coefficient. The correlation coefficient (*R*) provides the ability of the suggested models in predicting the bubble departure diameter data with values from 0 to 1. Based on Fig. 17, the *R* values of the regression diagrams for the bubble departure diameter are 0.96524 and 0.95754 for training and all datasets, respectively. Most of the data points for both test and validation are condensed near the line that indicates the precise estimation of the

suggested models. The *R* values for the bubble departure diameter using the 2HL network for the training and all datasets are 0.98918 and 0.98079, respectively. Also, based on Fig. 16, the *R* values for the training and all datasets 0.96091 and 0.96321. These results suggest that the MLP neural network with 2HL can accurately predict the bubble departure diameter in nucleate boiling from a heated surface. The developed ANN model enables the accurate prediction of the bubble departure diameter at different subcooling levels and wall temperatures.

Additionally, Figs. 20-22 show the error histogram for the bubble departure diameter with the 1HL, 2HL, and 3HL neural networks. The error histogram is a graph of the errors between target values and predicted values from the neural network. This indicates how predicted values are close to the target values, and how the errors from the neural network are distributed. For achieving a precise model, the error distribution diagram is needed to obey the normal distribution diagram. Based on Fig. 20, the errors are normally distributed and considerably low. In other words, the error frequency accumulates mainly in the zero-axis error range, which makes a symmetric graph and shows that the methods have an excellent performance in estimating the behavior of the bubble departure diameter. Note that the "zero error" line separates negative and positive values. The sign of the error shows the direction of

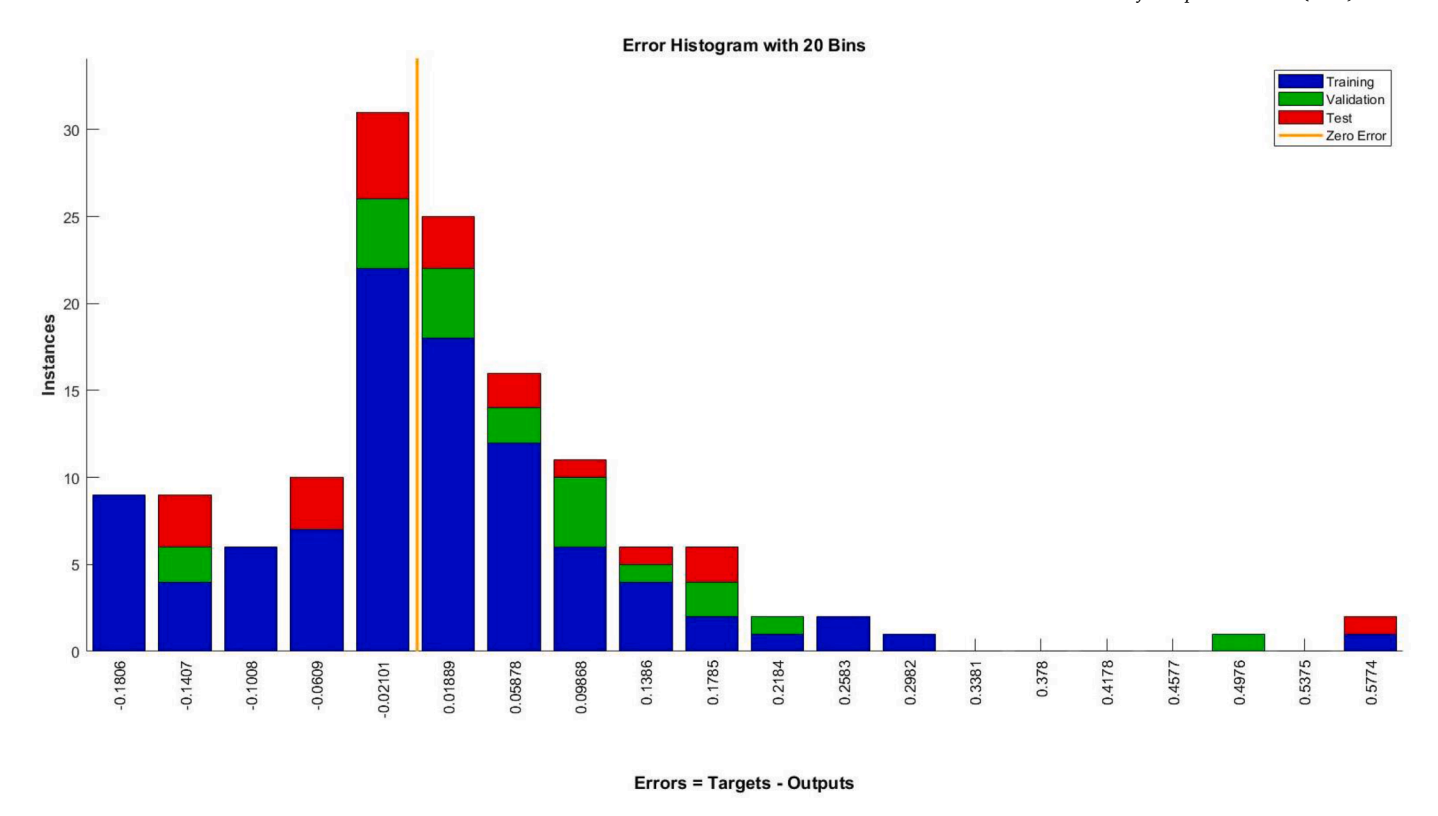


Fig. 20. Error analysis for bubble departure diameter with the 1HL network.

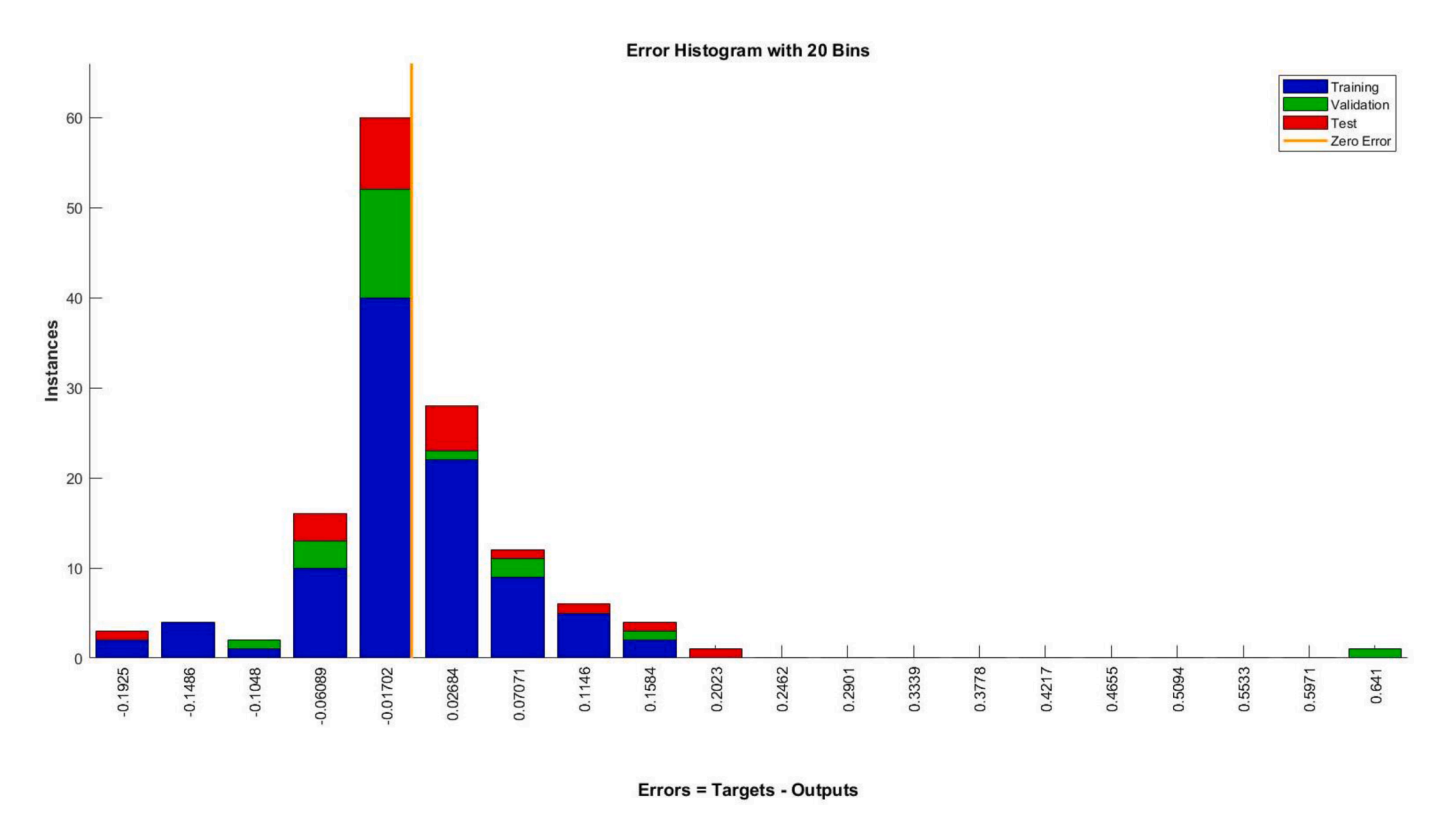


Fig. 21. Error analysis for bubble departure diameter with the 2HL network.

the bias. The positive error means the outputs are smaller than the targets, and the negative error means that the targets are larger than the outputs. Also, Fig. 23 shows the comparison between MSE and $\it R$ values for 1HL, 2HL, and 3HL neural networks. These results show that the

network with 2HL has the best performance and creates the least error.

The results of the study indicate that the use of the logsig transfer

The results of the study indicate that the use of the logsig transfer function on both hidden layers of the MLP neural network with three neurons on each hidden layer provides the best prediction performance

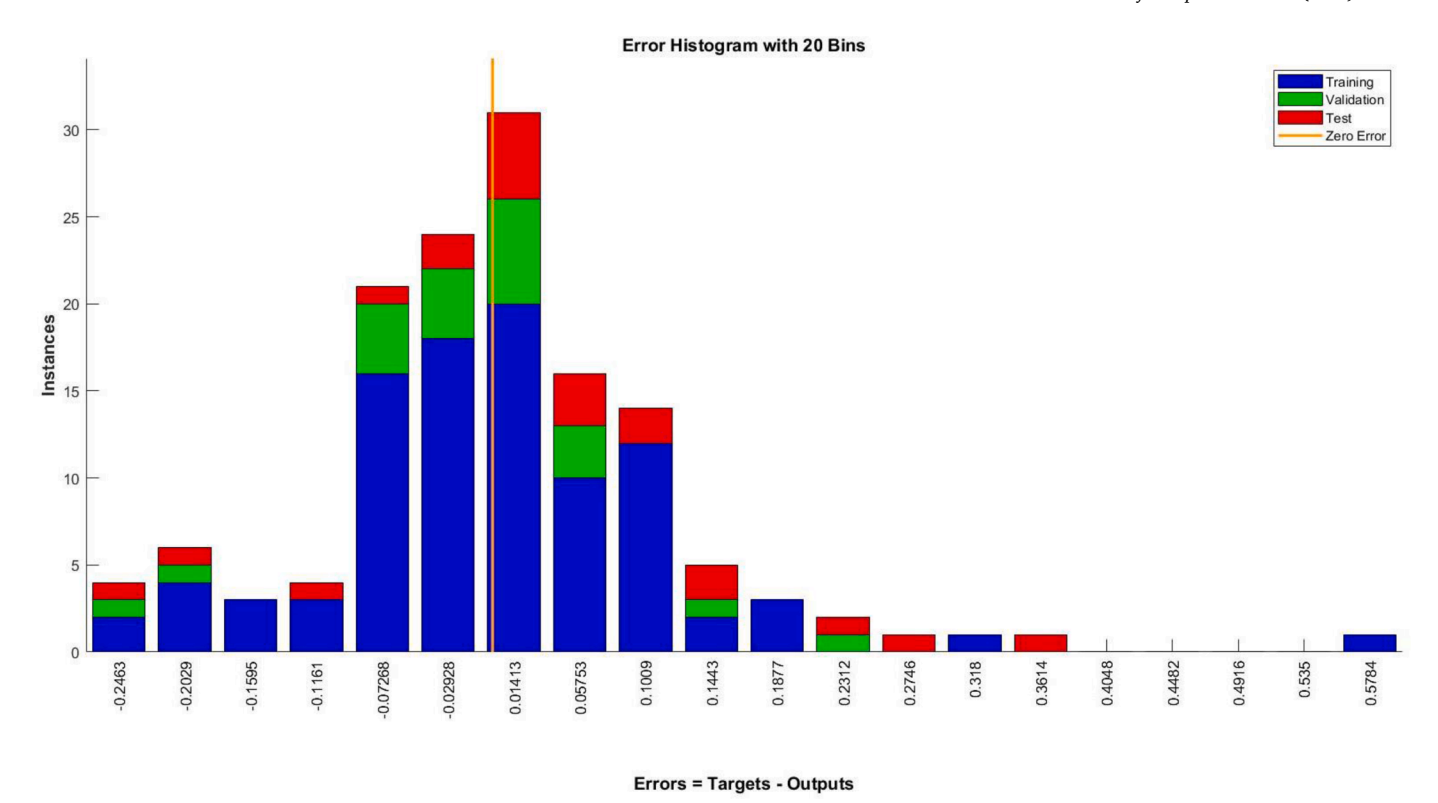


Fig. 22. Error analysis for bubble departure diameter with the 3HL network.

for the bubble departure diameter (Table 4). This is because the logsig transfer function can effectively handle non-linear relationships between input and output variables, which is important in bubble dynamics since the relationship between the input parameters (wall superheat and subcooling level) and the output parameter (bubble departure diameter) is non-linear. Using a non-linear transfer function like logsig can better capture and model these non-linear relationships. Furthermore, the logsig transfer function has a smooth gradient, making it easier to adjust the weights of the connections between neurons during the backpropagation training process. This allows for faster and more efficient training of the neural network, resulting in more accurate predictions of the bubble departure diameter. These optimal values of the design parameters can serve as a guideline for other researchers who want to use MLP neural networks to predict bubble departure diameter in similar boiling systems. However, it is important to note that the optimal values may differ depending on the specific characteristics of the boiling system and the data used for training the neural network.

4. Conclusion

This work investigates the heat transfer performance of two fin structures, namely regular and modified fins, in a pool boiling facility. The modified fin structure enhances the regular fin's heat transfer performance by adding an additional artificial nucleation site. With fin heat sinks, different bubble dynamics parameters, such as bubble departure diameter and bubble growth rate, are visualized and examined using high-speed optical imaging. Pool boiling experiments estimate heat transfer rates and coefficients in atmospheric pressure conditions using deionized water. Also, a multilayer perceptron ANN with a back-propagation training algorithm is applied for modeling the bubble departure diameter at different wall superheat and subcooling levels. The mean square error of the model is calculated to evaluate the accuracy of the models. This approach would help understand the bubble behavior in nucleate boiling and, consequently, achieve a universal theoretical prediction of bubble growth in boiling. In summary

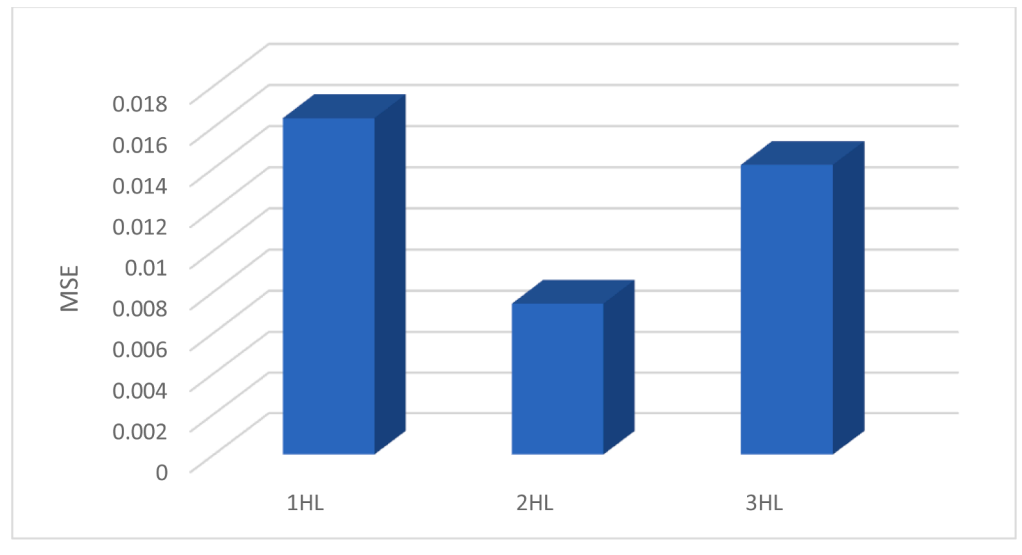
- The modified fin shows better heat transfer performance than the regular fin, with a higher bubble departure diameter and growth rate.
- 2) The local wall temperature in the modified fin is lower because the rapid bubble nucleation takes away large amounts of heat at a higher bubble frequency thanks to the artificial nucleation site.
- 3) The bubble departure diameter for the modified fin is 29% larger than the regular fin at a subcooling level of 10 $^{\circ}\text{C}$ and wall superheat of 6 $^{\circ}\text{C}$.
- 4) The MLP neural network can accurately predict the bubble departure diameter in nucleate boiling from a heated surface. The results show that the network with 2HL has the least error and can predict the desired parameter with a precision of 0.98079. Moreover, the modeling results show that the residuals are scattered around the zero axis, which shows the model's accuracy.
- 5) By comparing the two fin surfaces, the surface with an artificial nucleation site shows a lower wall temperature at the same heat flux. It can be found that in the convection boiling region, there is no significant difference between the wall temperatures for both surfaces. The heat transfer performance of the modified fin is better than the regular fin in the nucleate boiling region.

CRediT authorship contribution Statements

Mahyar Ghazvini: Conceptualization, Design, Optimization, Experiments, Data Analysis, Writing, Editing. **Mazen Hafez**: Experiments, Data Analysis. **Philippe Mandin**: Data Review, Editing. **Myeongsub Kim**: Conceptualization, Design, Data Analysis, Writing, Editing, Review.

Declaration of Competing Interest

The authors declare that there are no conflicts of interest.



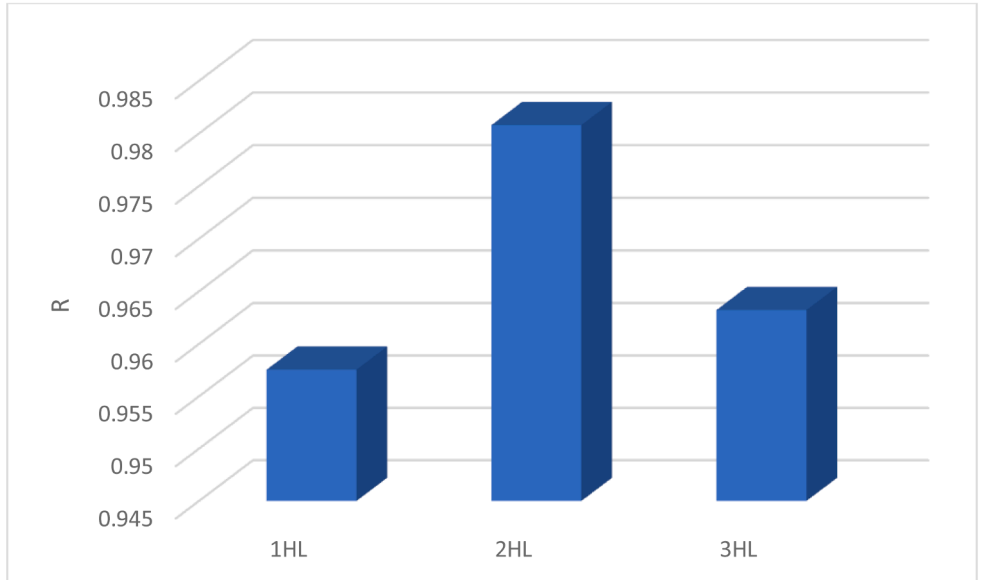


Fig. 23. Comparison between MSE and R values for 1HL, 2HL, and 3HL networks.

Table 4Optimum values of the design parameters for the bubble departure diameter with the 2HL network.

 N _i (number of neurons)		F _i (transfe	F _i (transfer function)	
 N_1	N_2	F_1	F ₂	
 3	3	logsig	logsig	0.007403

Data availability

Data will be made available on request.

Acknowledgment

This work was financially supported by the National Science Foundation (#1917272).

References

Bertossi, R., Caney, N., Gruss, J.A., Poncelet, O., 2015. Pool boiling enhancement using switchable polymers coating. Appl. Therm. Eng. 77, 121–126. https://doi.org/10.1016/J.APPLTHERMALENG.2014.11.061.

Chu, K.H., Enright, R., Wang, E.N., 2012. Structured surfaces for enhanced pool boiling heat transfer. Appl. Phys. Lett. 100, 241603 https://doi.org/10.1063/1.4724190.

Cole, R., Shulman, H.L., 1966. Bubble growth rates at high Jakob numbers. Int. J. Heat Mass Transf. 9, 1377–1390. https://doi.org/10.1016/0017-9310(66)90135-9.

Ertuğrul, Ö.F., 2018. A novel type of activation function in artificial neural networks: Trained activation function. Neural Networks 99, 148–157. https://doi.org/10.1016/j.neunet.2018.01.007.

Fan, L.W., Li, J.Q., Li, D.Y., Zhang, L., Yu, Z.T., Cen, K.F., 2015. The effect of concentration on transient pool boiling heat transfer of graphene-based aqueous nanofluids. Int. J. Therm. Sci. 91, 83–95. https://doi.org/10.1016/J. IJTHERMALSCI.2015.01.009.

Fazel, S.A., S.S.-J. of heat, undefined, 2010. Bubble dynamics for nucleate pool boiling of electrolyte solutions. Asmedigitalcollection.Asme.Org. (n.d.). https://asmedigital collection.asme.org/heattransfer/article-abstract/132/8/081502/458418. accessed January 16, 2020.

Forster, H.K., Zuber, N., 1954. Growth of a vapor bubble in a superheated liquid. J. Appl. Phys. 25, 474–478. https://doi.org/10.1063/1.1721664.

Ghazivini, M., Hafez, M., Ratanpara, A., Kim, M., 2021. A review on correlations of bubble growth mechanisms and bubble dynamics parameters in nucleate boiling. J. Therm. Anal. Calorim. 2021. 1–37. https://doi.org/10.1007/S10973-021-10876-2

Ghazvini, M., Delius, R., Richards, S., Ratanpara, A., Hafez, M., Kim, M., 2021. Experimental Study of Pool Boiling Heat Transfer on Novel Pin-Finned Surfaces.

- APS. N01.122. https://ui.adsabs.harvard.edu/abs/2021APS..DFDN01122G/abstract (accessed September 7, 2022).
- Ghazvini, M., Maddah, H., Peymanfar, R., Ahmadi, M.H., Kumar, R., 2020. Experimental evaluation and artificial neural network modeling of thermal conductivity of water based nanofluid containing magnetic copper nanoparticles. Phys. A Stat. Mech. Its Appl., 124127 https://doi.org/10.1016/j.physa.2019.124127.
- Hamzekhani, S., Falahieh, M.M., Kamalizadeh, M.R., Nazari, Z., 2015. Experimental study on bubble departure frequency for pool boiling of water/NaCl solutions. Heat Mass Transf. Und Stoffuebertragung 51, 1313–1320. https://doi.org/10.1007/s00231_015_1502_x
- Hashemi, A., Jang, J., 2023. Smart Active Vibration Control System of a Wind Turbine Blade Using Piezoelectric. Material 1–15. https://doi.org/10.1007/978-3-031-05440-5-1
- Hashemi, A., Jang, J., Hosseini-Hashemi, S., 2022. Semi-Analytical Analysis for Dynamic Behaviors of Wind Turbine Blades Using Transfer Function Methods. Conf. Proc. Soc. Exp. Mech. Ser. 33–43. https://doi.org/10.1007/978-3-030-75996-4_5/COVER.
- Herzog, S., Tetzlaff, C., Wörgötter, F., 2020. Evolving artificial neural networks with feedback. Neural Networks 123, 153–162. https://doi.org/10.1016/j.neunet 2019.12.004
- Honda, H., Takamatsu, J.J.Wei, 2003. Enhanced Boiling Heat Transfer from Silicon Chips with Micro-Pin Fins Immersed in FC-72. J. Enhanc. Heat Transf. 10, 211–223. https://doi.org/10.1615/JENHHEATTRANSF.V10.12.70.
- Honda, H., Wei, J.J., 2004. Enhanced boiling heat transfer from electronic components by use of surface microstructures. Exp. Therm. Fluid Sci. 28, 159–169. https://doi. org/10.1016/S0894-1777(03)00035-9.
- Kim, J., Jun, S., Lee, J., Godinez, J., You, S.M., 2017. Effect of Surface Roughness on Pool Boiling Heat Transfer of Water on a Superhydrophilic Aluminum Surface. J. Heat Transfer. 139. https://doi.org/10.1115/1.4036599/384231.
- Markal, B., Aydin, O., Avci, M., 2017. Prediction of Heat Transfer Coefficient in Saturated Flow Boiling Heat Transfer in Parallel Rectangular Microchannel Heat Sinks. An Experimental Study 38, 1415–1428. https://doi.org/10.1080/ 01457632.2016.1255038, 10.1080/01457632.2016.1255038.
- Markal, B., Candan, A., Aydin, O., Avci, M., 2018. Experimental investigation of flow boiling in single minichannels with low mass velocities. Int. Commun. Heat Mass Transf. 98, 22–30. https://doi.org/10.1016/J. ICHEATMASSTRANSFER.2018.08.002.
- Markal, B., Kul, B., 2022. Combined influence of artificial nucleation site and expanding cross section on flow boiling performance of micro pin fins. Int. Commun. Heat Mass Transf. 135, 106081 https://doi.org/10.1016/J. ICHEATMASSTRANSFER.2022.106081.
- Markal, B., Kul, B., Avci, M., Varol, R., 2022. Effect of gradually expanding flow passages on flow boiling of micro pin fin heat sinks. Int. J. Heat Mass Transf. 197, 123355 https://doi.org/10.1016/J.IJHEATMASSTRANSFER.2022.123355.
- Mei, Y., Shao, Y., Gong, S., Zhu, Y., Gu, H., 2018. Effects of surface orientation and heater material on heat transfer coefficient and critical heat flux of nucleate boiling. Int. J. Heat Mass Transf. 121, 632–640. https://doi.org/10.1016/J. IJHEATMASSTRANSFER.2018.01.020.
- Menni, Y., Ghazvini, M., Ameur, H., Kim, M., Ahmadi, M.H., Sharifpur, M., 2020. Combination of baffling technique and high-thermal conductivity fluids to enhance

- the overall performances of solar channels. Eng. with Comput 381 (38), 607–628. https://doi.org/10.1007/S00366-020-01165-X, 2020.
- Mikic, B.B., Rohsenow, W.M., 1969. A new correlation of pool-boiling data including the effect of heating surface characteristics. J. Heat Transfer. 91, 245–250. https://doi. org/10.1115/1.3580136.
- Mikic, B.B., Rohsenow, W.M., Griffith, P., 1970. On bubble growth rates. Int. J. Heat Mass Transf. 13, 657–666. https://doi.org/10.1016/0017-9310(70)90040-2.
- Mourgues, A., Hourtané, V., Muller, T., Caron-Charles, M., 2013. Boiling behaviors and critical heat flux on a horizontal and vertical plate in saturated pool boiling with and without ZnO nanofluid. Int. J. Heat Mass Transf. 57, 595–607. https://doi.org/10.1016/j.ijheatmasstransfer.2012.10.073.
- Pioro, I.L., 1999. Experimental evaluation of constants for the Rohsenow pool boiling correlation. Int. J. Heat Mass Transf. 42, 2003–2013. https://doi.org/10.1016/ S0017-9310(98)00294-4.
- Qiu, Y., Garg, D., Zhou, L., Kharangate, C.R., Kim, S.M., Mudawar, I., 2020. An artificial neural network model to predict mini/micro-channels saturated flow boiling heat transfer coefficient based on universal consolidated data. Int. J. Heat Mass Transf. 149, 119211 https://doi.org/10.1016/J.IJHEATMASSTRANSFER.2019.119211.
- Rini, D.P., Chen, R.H., Chow, L.C., 2002. Bubble behavior and nucleate boiling heat transfer in saturated FC-72 spray cooling. J. Heat Transfer. 124, 63–72. https://doi. org/10.1115/1.1418365.
- Sayed, A., Sardeshmukh, M., Limkar, S., 2014. Optimisation Using Levenberg-Marquardt Algorithm of Neural Networks for Iris. Adv. Intell. Syst. Comput., Springer Verlag 91–98. https://doi.org/10.1007/978-3-319-02931-3_12.
- Tang, J., Sun, L., Wu, D., Du, M., Xie, G., Yang, K., 2019. Effects of ultrasonic waves on subcooled pool boiling on a small plain heating surface. Chem. Eng. Sci. 201, 274–287. https://doi.org/10.1016/j.ces.2019.03.009.
- Wei, J.J., Honda, H., 2003. Effects of fin geometry on boiling heat transfer from silicon chips with micro-pin-fins immersed in FC-72. Int. J. Heat Mass Transf. 46, 4059–4070. https://doi.org/10.1016/S0017-9310(03)00226-6.
- Xue, Y.F., Zhao, J.F., Wei, J.J., Zhang, Y.H., Qi, B.J., 2013. Experimental study of nucleate pool boiling of FC-72 on micro-pin-finned surface under microgravity. Int. J. Heat Mass Transf. 63, 425–433. https://doi.org/10.1016/J. LJHEATMASSTRANSFER.2013.03.083.
- Yajima, S., Io, N., Miyazaki, K., Yabuki, T., 2022. Heat flux partitioning and macrolayer observation in pool boiling of water on a surface with artificial nucleation sites. Int. J. Heat Mass Transf. 194, 122924 https://doi.org/10.1016/J. LJHEATMASSTRANSFER.2022.122924.
- Zhang, B.J., Kim, K.J., 2014. Nucleate pool boiling heat transfer augmentation on hydrophobic self-assembly mono-layered alumina nano-porous surfaces. Int. J. Heat Mass Transf. 73, 551–561. https://doi.org/10.1016/J. LJHEATMASSTRANSFER.2014.02.032.
- Zhang, Y., Ma, X., Zhu, Z., Duan, L., Wei, J., 2021. Critical heat flux prediction model of pool boiling heat transfer on the micro-pillar surfaces, Case Stud. Therm. Eng. 28, 101668 https://doi.org/10.1016/J.CSITE.2021.101668.
- Zhou, J., Xu, P., Qi, B., Zhang, Y., Wei, J., 2022. Effects of micro-pin-fins on the bubble growth and movement of nucleate pool boiling on vertical surfaces. Int. J. Therm. Sci. 171, 107186 https://doi.org/10.1016/J.IJTHERMALSCI.2021.107186.